JOURNAL OF GEOPHYSICAL RESEARCH, VOL. 115, C06007, doi:10.1029/2009JC005383, 2010

Vortical surf zone velocity fluctuations with 0(10) min period

Jamie H. MacMahan,[1] Ad J. H. M. Reniers,[2,3] and Ed B. Thornton[1]

Received 13 March 2009; revised 30 October 2009; accepted 19 January 2010; published 10 June 2010.

[1] Observations of velocity fluctuations with periods between about 4 and 30 min, thus longer than infragravity waves and referred to as very low frequency (VLF) surf zone motions, are described and compared with numerical simulations. The VLF motions discussed here exclude instabilities (generated by the wave-driven alongshore current velocity shear) that occur in the same frequency range by selecting cases with weak alongshore currents only. Numerical simulations are based on the linear shallow water equations including friction and forced by nonlinear difference-frequency interactions between incident sea and swell waves. The model is initialized with sea and swell frequency directional spectra observed seaward of the surf zone. Modeled and observed VLF velocity fluctuation magnitudes agree within a factor of 2; both increase approximately linearly with increasing incident wave height and rapidly decay seaward of the surf zone. Observed frequency-wave-number, f-k_y, spectra of VLF velocity fluctuations, estimated with instrumented alongshore arrays, are energetic in a broad range of k_y in the vortical band. Observed and modeled VLF pressure fluctuations are relatively weak. Still, the model momentum balance suggests that VLF pressure gradients are as important as the nonlinear wave group forcing by sea and swell in accelerating/decelerating the VLF velocities. Model calculations demonstrate that the VLF-f-k_y response is a function of the modulations of short-wave forcing associated with the frequency directional distribution of the incident sea and swell spectra. This results in VLF motions which span the surf zone and have O(50–1000 m) alongshore scales with O(200–2000 s) time scales. Given the fact that modulations of short waves resulting from directionally spread incident waves are common during field conditions we expect VLFs to be ubiquitous.

Citation: MacMahan, J. H., A. J. H. M. Reniers, and E. B. Thornton (2010), Vortical surf zone velocity fluctuations with 0(10) min period, *J. Geophys. Res.*, *115*, C06007, doi:10.1029/2009JC005383.

1. Introduction

[2] Shoaling and breaking swell and sea waves (with periods less than about 25 s) drive surf zone velocity fluctuations with longer periods. These motions include infragravity waves with periods in the range of 25 s to 250 s [*Munk*, 1949; *Tucker*, 1950], shear instabilities with periods in the range of 1 to 10 min [*Oltman-Shay et al.*, 1989], and wave breaking induced vortical motions with periods in the range of 4 to 30 min [*Ryrie*, 1983; *Tang and Dalrymple*, 1989; *Peregrine*, 1998, 1999; *MacMahan et al.*, 2004].

[3] Given their overlap in temporal scales discriminating between infragravity waves, shear instabilities and breaking induced vortices is not trivial in frequency (f) space. This problem is overcome by including the alongshore length scales associated with these motions described by alongshore wave number (k_y) spectra. The energy associated with infragravity waves resides inside the gravity region of f-k_y spectra defined by $|f/k_y| > \sqrt{gh}$. This separates the infragravity waves from the shear instabilities and breaking induced vortical motions which both reside in the vortical region of f-k_y space, where $|f/k_y| < \sqrt{gh}$. Shear instability energy density generated by the wave-driven alongshore current velocity shear is located on nondispersive ridges with propagation velocities in the order of the mean alongshore current velocity. With strong 0(1 m/s) mean alongshore currents, shear instabilities RMS velocity fluctuations can reach O(40 cm/s) [*Noyes et al.*, 2004]. During periods of near-normal wave incidence the alongshore currents and shear instabilities are weak, however significant energy can still be present in the vortical region with O(10 min) periods [e.g., *Tang and Dalrymple*, 1989]. These motions have been referred to as very low frequency motions (VLFs) by *MacMahan et al.* [2004] who observed energetic VLFs coupled to well-developed rip channel morphology, resulting in strong oscillations of the rip current flow with RMS velocity fluctuations reaching 40 cm/s.

[4] There is considerable evidence that wave groups made up of intersecting wave trains can generate strong vortical motions. This is based on laboratory experiments by *Fowler* [1991] and *Fowler and Dalrymple* [1990] showing that nonlinear difference interactions between two incident waves (frequencies f_1, f_2 and alongshore wave numbers $k_{1,y}, k_{2,y}$) can

[1]Oceanography Department, Naval Postgraduate School, Monterey, California, USA.
[2]Rosenstiel School of Marine and Atmospheric Science, University of Miami, Miami, Florida, USA.
[3]Department of Civil Engineering and Geosciences, Delft University of Technology, Delft, Netherlands.

0148-0227/10/2009JC005383

force detectable surf zone velocity fluctuations at $\Delta f = f_2 - f_1$ and $\Delta k_y = k_{2,y} - k_{1,y}$ regardless of whether Δf, Δk_y resides in the gravity or vortical region of f, k_y space.

[5] These laboratory results are supported by recent modeling studies. *Reniers et al.* [2004] modeled the nonlinear long-wave equations in the time domain forced by realistic directional wave spectra (large number of frequency directional components), resulting in random packets of wave energy formed by modulations of short waves (wave groups) entering the surf zone. As these modulations of short waves break within the surf zone, gradients in radiation stresses (momentum fluxes of sea and swell waves) and pressure are created, which force transient very low frequency surf zone eddies that have preferential alongshore spatial scales similar to the modulations of short waves (wave groups). We refer to wave groups as modulations of short waves because VLF surf zone response (eddies) occurs on the O(10 min) time scale, which is typically longer than wave groups that are commonly discussed in the literature that are associated with infragravity motions (IG), 30 s to 5 min. In essence, there are IG wave group modulations that travel on top of VLF wave group modulations. The general and most appropriate characterization for both sets of IG and VLF wave group modulations is short-wave modulations, which is used herein.

[6] *Reniers et al.* [2004, 2007] numerically found VLFs within the surf zone coupled to rip channel morphology, and obtained good agreement with field observations when modulations of short waves are included. *Johnson and Pattiaratchi* [2006] also modeled short-wave modulation forced circulation patterns associated with transient rip currents utilizing a Boussinesq model (FUNWAVE) [*Wei et al.*, 1995; *Kirby et al.*, 1998; *Kennedy et al.*, 2000; *Chen et al.*, 1999], and found similar results to *Reniers et al.* [2004]. *Johnson and Pattiaratchi* [2006] found that energetic peaks in the VLF band within the vortical region of f-k_y space were also present for a planar beach. *Long and Özkan-Haller* [2009] showed that the VLF response could be explained by constructive and destructive interference of short-wave modulated breaking induced vortices.

[7] However, field verification and understanding of VLFs on alongshore planar and barred beaches is incomplete. Part of this is due to the frequent coexistence and potential interaction of shear instabilities and wave breaking induced vortices masking the VLF response to the grouped incident waves. This was examined by *Haller et al.* [1999], who used SUPERDUCK86 field data to show that for obliquely incident waves the modulation of short wave forcing sometimes occurs at the time and spatial scales of free shear instabilities potentially leading to explosive growth of the shear instabilities [*Shira et al.*, 1997]. However, in many cases they failed to find coherent modulation of short wave forcing due to its broad distribution in k_y space. As a result traditional statistical tools are inadequate to explain the VLF response to broad modulations of short wave forcing. They also noted that in absence of shear instabilities a direct forced response is expected in the VLF range which was not explored further and is examined in detail here.

[8] To that end a shallow water spectral hydrodynamic model [*Reniers et al.*, 2002] is used to evaluate VLF motions during the SandyDuck Experiment at Duck, NC (1997), where extensive field observations of directional wave spectra, bathymetry, and five alongshore in situ pressure and velocity arrays are available. In the model, modulations of short waves made up of pairs of short-wave components, within a directionally spread wave field, with differences in Δf and Δk_y residing in the vorticity region of the f-k_y spectrum, which force a hydrodynamic response within the VLF band owing to radiation stress gradients within the surf zone. As a result, the VLF motions are expected to be a direct hydrodynamic response to that of the modulation of short waves forcing in f-k_y space. Consequently VLF motions are expected to be ubiquitous on natural beaches where frequency directionally spread short waves are incident.

2. Observations

[9] As part of the SandyDuck experiment, five alongshore arrays, 200m long, composed of six colocated pressure and electromagnetic current meters were deployed between about 50 and 300 m from the shoreline (Figure 1a) [*Elgar et al.*, 2001]. The alongshore variation of the beach profile over the instrumented region is weak [*Feddersen and Guza*, 2003], and the alongshore-averaged profile has weakly pronounced sand bars (Figure 1b). Offshore directional wave spectra were obtained in 8 m water depth using the method outlined by *Long and Atmadja* [1994].

[10] To eliminate cases with significant shear instability energy, cases are chosen with the mean alongshore currents $V < 25$ cm/s at each alongshore array. To eliminate cases with weak VLF energy, only cases with root-mean-square wave height $H_{RMS,8m} > 0.50$ m (in 8-m depth, referred to as the 8 m array) are retained. In the retained 75 3 h runs, $H_{RMS,8m}$ varied between 0.50–1.4 m, the mean wave period between 5–11 s, and the mean wave direction was between −9° to 13°. Retained runs were usually scattered throughout the experiment, with the exception of 18 retained runs during 13–15 November 1997.

3. Field Observations of VLFs

3.1. Spectral Analysis

[11] Estimates of f-k_y spectra were obtained for pressure (p) and the cross-shore (u) and alongshore (v) velocity components, using the maximum likelihood estimator (MLE) [*Regier*, 1975]. Spectral estimates with 10 degrees of freedom were generated from demeaned, quadratically detrended, 3 h records. The low degrees of freedom (and consequently large statistical scatter) is a consequence of the high resolution in frequency (0.0005 Hz) required to resolve VLF motions, and constraints on the record length (increasing the record length increases tidal and other nonstationarity).

[12] Results for the 3 h record with the most energetic VLF motions (0400 LT 14 November; Figure 2) are representative of other records, as similar f-k_y spectra were observed, but with less energy (not shown). For 0400 LT 14 November, all arrays shoreward of x = 400 m are considered to be within the surf zone, corresponding to a local $H_{RMS}/h > 0.3$ (Figure 3a). Dissipation owing to depth-limited wave breaking is most intense between 160 and 210 m in the cross shore and near the waterline. The maximum VLF vortical energy in the cross shore is located in these regions with the largest dissipation and concomitant radiation stress gradients.

[13] Peaks are observed within the vortical region of the VLF band in the u and v f-k_y spectra (Figure 2). VLFs travel

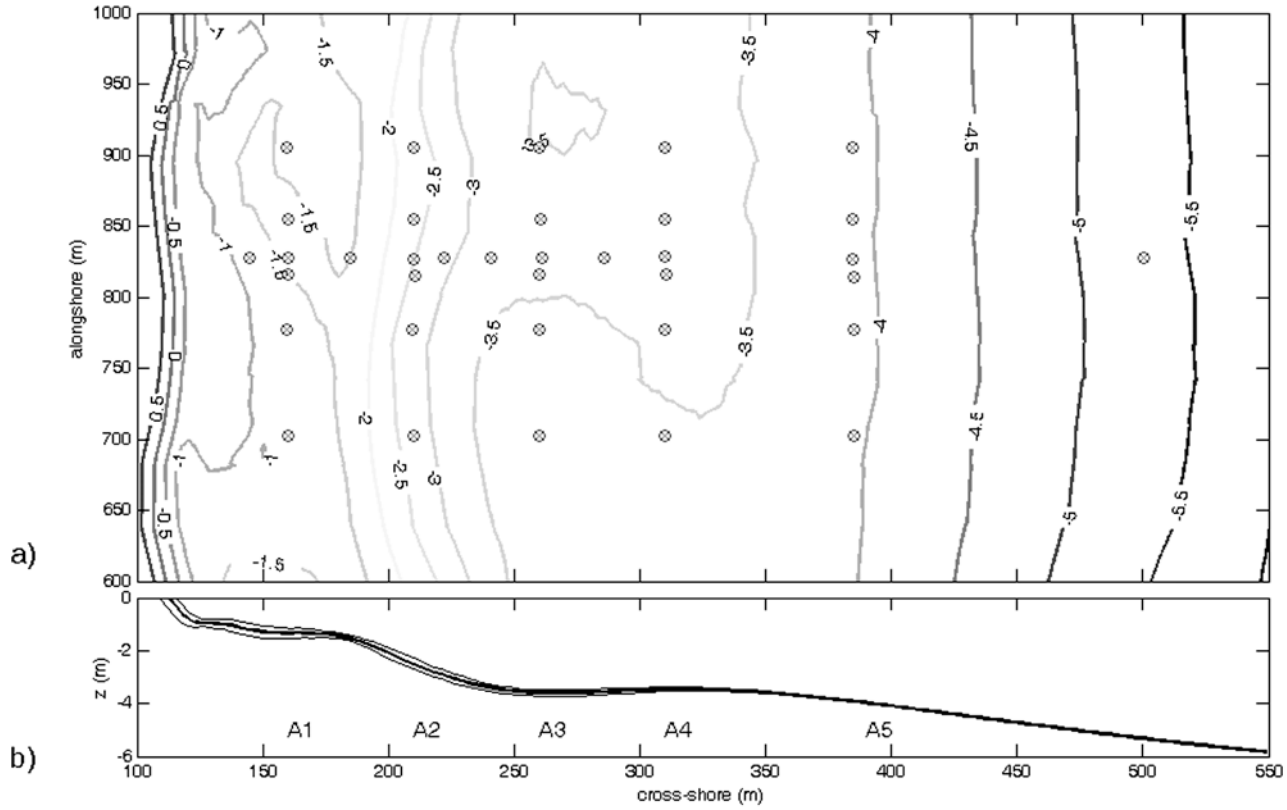

Figure 1. (a) Locations of colocated pressure and electromagnetic current meters (indicated with cross in a circle) are superimposed on bathymetry measured 30 October 1997 (depth contours are in m). (b) Seafloor elevation z versus cross-shore coordinate. The average of 10 cross-shore transects is shown with a bold curve, and the thin curves indicate plus and minus 1 standard deviation. Alongshore arrays of instruments are denoted A1–A5, with A1 most shoreward. The Field Research Facility coordinate frame is used.

both up and down coast. For an alongshore wave number of 0.01 m^{-1} and a frequency of 0.002 Hz (Figure 2 (top), A1), the corresponding propagation velocity is 0.2 m/s. With an average life time of 10 min this means that VLFs can propagate O(100) m alongshore, consistent with the results of *Long and Özkan-Haller* [2009]. VLF energy density decreases at higher frequencies within the vortical region. VLF energy is largest at the inner two arrays (A1 and A2), where maximum dissipation occurs, and decreases offshore (Figures 2, 3b, and 3c). The corresponding sea surface elevation energy density is concentrated within the gravity region with negligible VLF energy in the vorticity region (Figure 2). The spectral distributions shown in Figure 2 are typical for other 3 h events.

3.2. Bulk Statistics

[14] A total VLF flow magnitude $q_{RMS,vlf}$ is estimated by integrating the sum of the cross-shore ($G_{uu}(f, k_y)$) and alongshore ($G_{vv}(f, k_y)$) velocity spectra within the vorticity region of f-k_y space

$$q^2_{RMS,vlf} = \int_{-0.04m^{-1}}^{-k_{yg}} \int_{0.0005Hz}^{0.004Hz} \left[G_{uu}(f,k_y) + G_{vv}(f,k_y)\right] df dk_y + \int_{k_{yg}}^{0.04m^{-1}} \int_{0.0005Hz}^{0.004Hz} \left[G_{uu}(f,k_y) + G_{vv}(f,k_y)\right] df dk_y, \quad (1)$$

where $k_{yg} = f/\sqrt{gh}$. In general, $q_{RMS,vlf}$ increases with increasing $H_{RMS,8m}$ and with increasing proximity to the shoreline (Figure 4a). The $q_{RMS,vlf}$ is larger in the surf zone and decreases seaward. At array A1, always within the surf zone, $q_{RMS,vlf}$ increases approximately linearly with $H_{RMS,8m}$.

[15] Defining the outer limit of the surf zone as the most seaward point where $H_{RMS,8m} < 0.3$ h, the most energetic VLFs (solid symbols) occur when the alongshore array is within the surf zone. The $q_{RMS,vlf}$ of the inner alongshore array (x = 160 m, circles) increases with wave height, with a slope of approximately one in the surf zone and much less outside of the surf zone. $q_{RMS,vlf}$ of the second alongshore array (x = 210 m, squares) also increases strongly with increasing wave height, provided it is located within the surf zone, and its maximum magnitude is approximately half of the inner array's magnitude. $q_{RMS,vlf}$ of the remaining offshore alongshore arrays increase with increasing $H_{RMS,8m}$, but are much smaller in magnitude compared with inner array's $q_{RMS,vlf}$. The maximum $q_{RMS,vlf}$ is approximately 20 cm/s for the shore-normal incident wave conditions considered here. $q_{RMS,vlf}$ is approximately the same magnitude as $q_{RMS,ig}$ (Figure 4b), which also increases with increasing wave energy [e.g., *Holman*, 1981; *Guza and Thornton*, 1985; *Lippmann et al.*, 1999].

[16] In summary, VLFs are found during normally incident waves, maximum within the surf zone (limited in the offshore extent), related to the incoming wave height based on the field

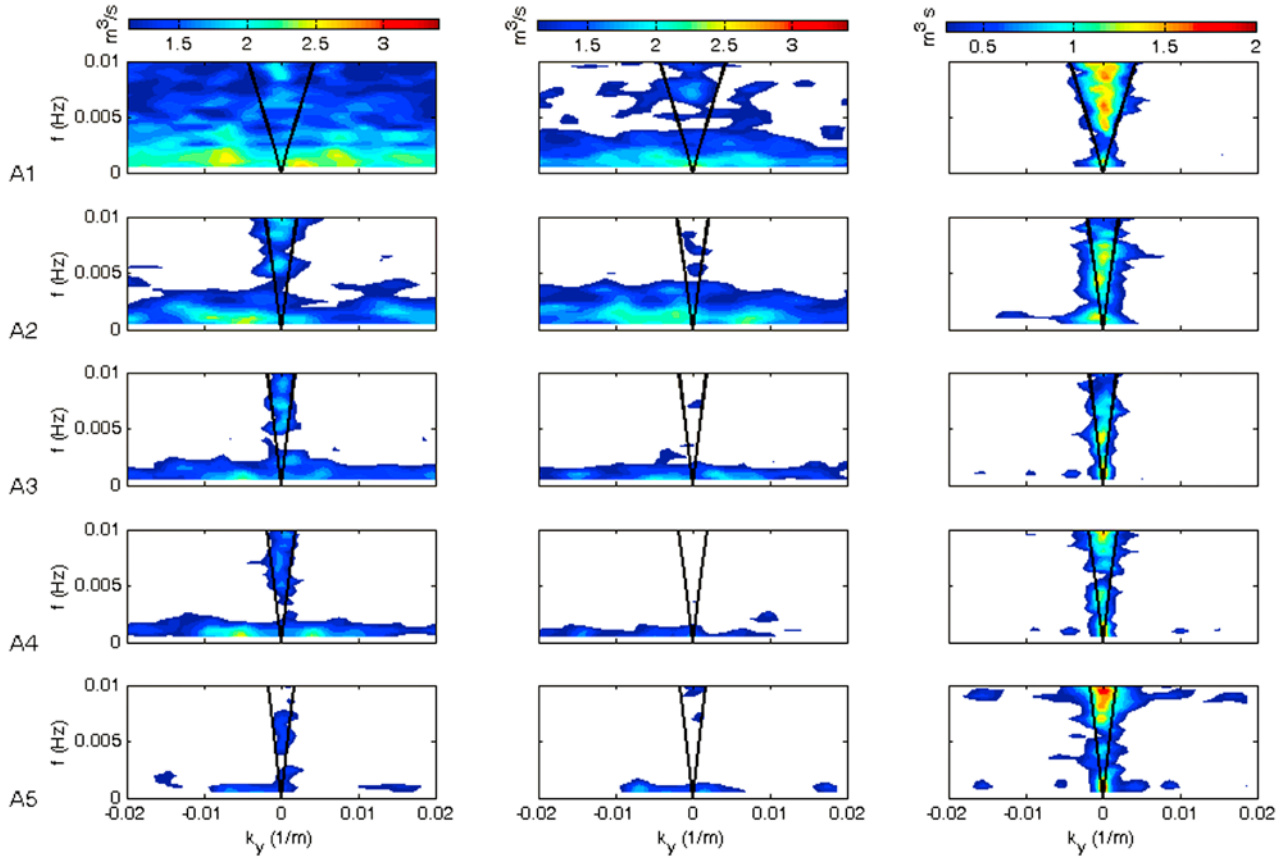

Figure 2. Frequency-alongshore-wave-number f-k_y spectra of (left) cross-shore velocity u, (middle) alongshore velocity v, and (right) pressure p. This 3 h run (0400 LT 14 November 1997) had the largest incident waves of any retained run ($H_{RMS,8m}$ = 1.41 m, T_{mean} = 7 s and θ_{mean} = −3°). Shallowest (A1) and deepest (A5) arrays are at the top and bottom, respectively. Bold lines are $k_y = f/\sqrt{gh}$. Color scales are at the top.

observations, and have magnitudes equivalent to IG motions with similar forcing.

4. VLF Model Description

[17] A shallow water spectral hydrodynamic model by *Reniers et al.* [2002] is used to evaluate the VLF forcing. The model approximates the bathymetry as alongshore homogeneous and lateral hydrodynamic boundary conditions as alongshore periodic. Model inputs are an offshore directional wave spectrum (Appendix A) and a beach profile. *Reniers et al.* [2002] verified that the model produces good results of sea surface elevation within the IG band, η_{ig}. The model is used here to investigate η, u, and v within the VLF band.

[18] The linearized, depth and short-wave-averaged shallow water equations [*Phillips*, 1977] are used by *Reniers et al.* [2002] to describe the hydrodynamic response for slowly varying short-wave modulation. The continuity equation is given by

$$\frac{\partial \eta}{\partial t} + \frac{\partial hu}{\partial x} + \frac{\partial hv}{\partial y} = 0, \tag{2}$$

with a right-handed coordinate system, where x is positive onshore, and h is the total water depth including wave setup. The cross-shore and alongshore momentum balances are

$$\frac{\partial u}{\partial t} + g\frac{\partial \eta}{\partial x} = -F^x - \tau_x, \tag{3}$$

$$\frac{\partial v}{\partial t} + g\frac{\partial \eta}{\partial y} = -F^y - \tau_y, \tag{4}$$

where the forcing terms (F^x, F^y) are

$$F^x = \frac{1}{\rho h}\left(\frac{\partial S_{xx}}{\partial x} + \frac{\partial S_{xy}}{\partial y}\right), \tag{5}$$

$$F^y = \frac{1}{\rho h}\left(\frac{\partial S_{yy}}{\partial y} + \frac{\partial S_{yx}}{\partial x}\right), \tag{6}$$

where S_{xx}, S_{xy} and S_{yy} are components of the short-wave radiation stress tensor. The linearized bottom stresses

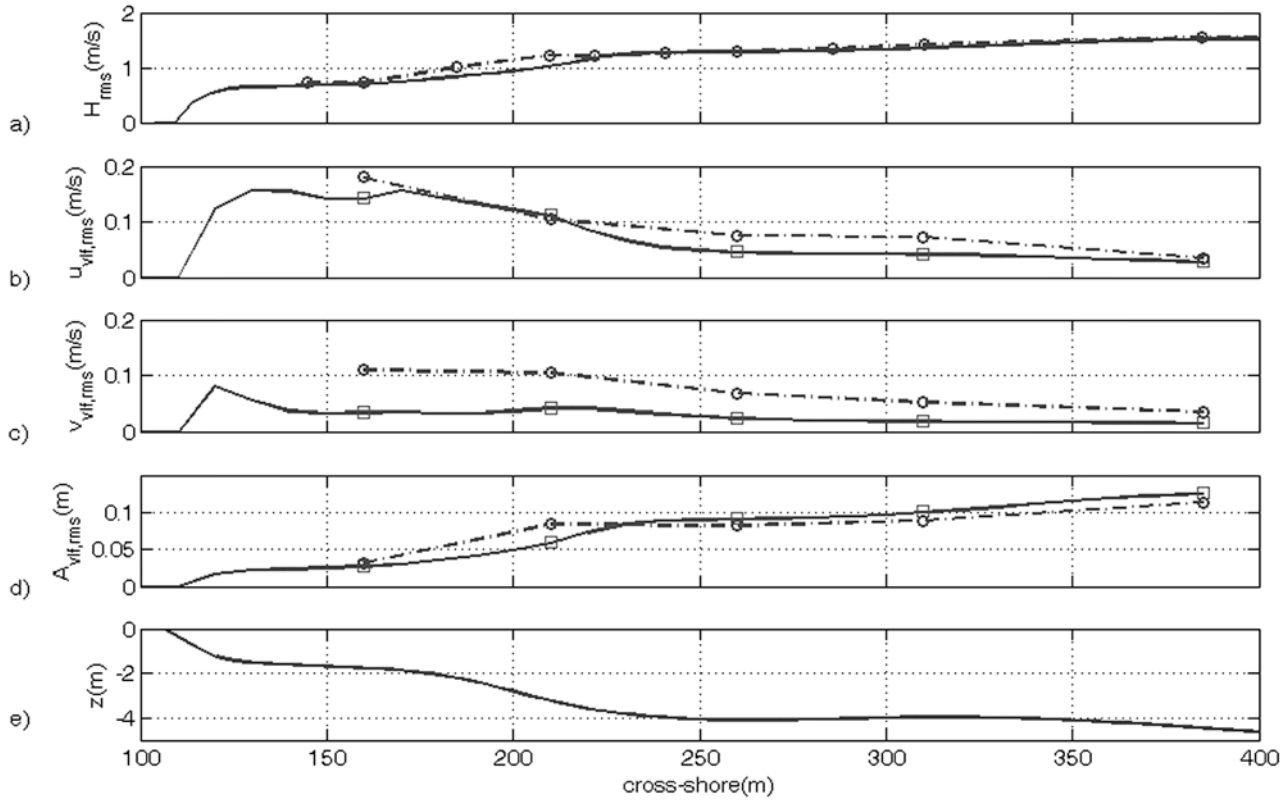

Figure 3. Modeled (solid line) and observed (dash-dotted line) (a) H_{RMS}, (b) $u_{RMS,vlf}$, (c) $v_{RMS,vlf}$, (d) $A_{RMS,vlf}$, and (e) observed depth versus cross-shore distance for 0400 LT 14 November 1997.

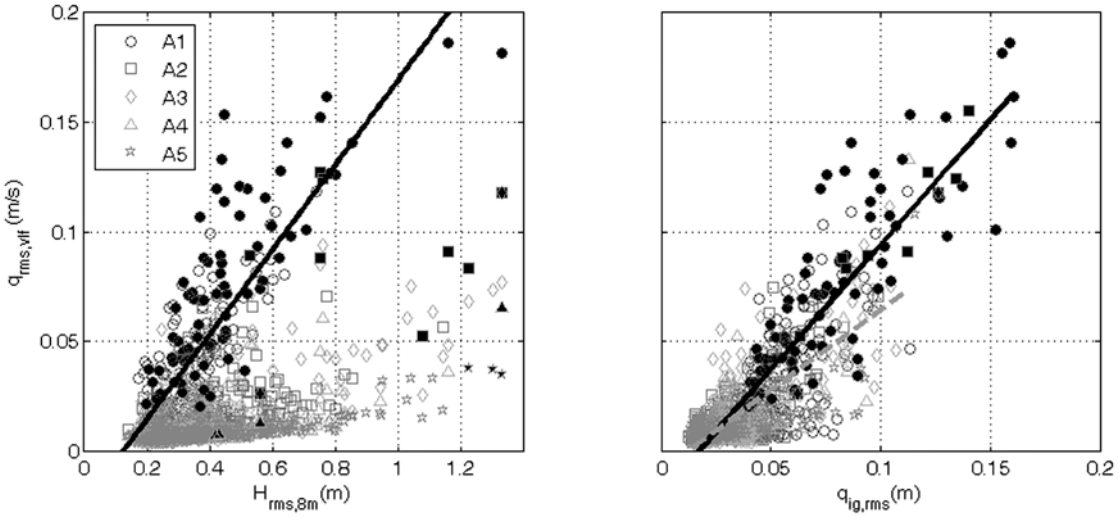

Figure 4. (left) RMS VLF velocity $q_{RMS,vlf}$ versus incident wave height H_{RMS} for 75 alongshore current shear instabilities free, 3 h runs, at each array (see legend). (right) The $q_{RMS,vlf}$ versus RMS IG velocity $q_{RMS,ig}$. The solid and open symbols indicate measurements within the surf zone ($H_{RMS}/h > 0.3$) and outside the surf zone ($H_{RMS}/h < 0.3$), respectively. In Figure 4 (left) the solid line is a linear regression for observations in the surf zone ($r^2 = 0.7$, m = 0.2). In Figure 4 (right) the solid line and dashed line are a linear regressions for observations in the surf zone ($r^2 = 0.7$, m = 1.1) and outside of the surf zone (m = 0.7, $r^2 = 0.6$).

(τ_x, τ_y) are [*Thornton and Guza*, 1986; *Özkan-Haller and Li*, 2003]

$$\tau_x = \mu \frac{u}{h}, \tag{7}$$

$$\tau_y = \mu \frac{v}{h}, \tag{8}$$

with μ

$$\mu = \frac{2}{\pi} c_f u_{sw}, \tag{9}$$

where c_f is the friction coefficient, and the short-wave orbital velocity (u_{sw}) obtained with linear wave theory is

$$u_{sw} = \frac{H_{RMS}}{2\sqrt{2}} \frac{2\pi f_{peak}}{\sin h\left(k_{peak} h\right)}, \tag{10}$$

where H_{RMS} is the local short-wave height.

[19] Wave forcing (equations (5) and (6)) is determined by the short-wave frequency directional spectrum. The equations for the response are linear, so the contribution of each short-wave pair can be computed independently. Short-wave component pairs are composed of different frequencies, f_i, and wave numbers, $k_{y,i}$, corresponding to the modulated component direction, α_i, which results in a slow modulation in the radiation stresses [*Schäffer*, 1993; *Reniers et al.*, 2002] that are periodic in time and the alongshore direction, defined as $S_{xx}(x, y, t, f_1, f_2, k_{y,1}, k_{y,2})$

$$= \frac{1}{2} \hat{S}_{xx}\left(x, f_1, f_2, k_{y,1}, k_{y,2}\right) \exp\left[i\left(2\pi \triangle f t - \triangle k_y y\right)\right] + *, \tag{11}$$

where the hat indicates the complex amplitude term, * indicates complex conjugate, and $\hat{S}_{xy}$, and $\hat{S}_{yy}$ are defined similarly. $\hat{S}_{ij}$ are defined in terms of incident waves in Appendix B, where i and j represent x and y.

[20] Radiation stresses are computed from the cross-shore variation of short-wave, $\hat{E}_w$, and roller, $\hat{E}_r$, energy modulation (Appendix B). The short-wave energy modulation balance is defined as

$$\frac{d\hat{E}_w\left(x, f_1, f_2, k_{y,1}, k_{y,2}\right) c_g \cos(\hat{\alpha})}{dx} = -\hat{D}_w\left(x, f_1, f_2, k_{y,1}, k_{y,2}\right), \tag{12}$$

where $\hat{D}_w$ is the energy dissipation of the short-wave energy modulation, c_g is the group velocity at the peak frequency of the short-wave spectrum, and $\hat{\alpha}$ is modulated direction, defined as

$$\hat{\alpha} = atan\left(\frac{k_{y,1} + k_{y,2}}{k_{x,1} + k_{x,2}}\right), \tag{13}$$

obtained with Snells' law. The cross-shore roller energy modulation is obtained by a roller energy balance [*Nairn et al.*, 1990; *Stive and de Vriend*, 1994]

$$2\frac{d\hat{E}_r\left(x, f_1, f_2, k_{y,1}, k_{y,2}\right) c\left(f_p\right) \cos(\hat{\alpha})}{dx} = \hat{D}_w\left(x, f_1, f_2, k_{y,1}, k_{y,2}\right) - \hat{D}_r\left(x, f_1, f_2, k_{y,1}, k_{y,2}\right), \tag{14}$$

where c is the wave celerity at the peak wave frequency, and $\hat{D}_r$ is the dissipation of the roller energy modulation and $\hat{D}_w$ acts as a source term. Dissipation formulations for modulated wave and roller energy are described by *Reniers et al.* [2002] and *Reniers and Battjes* [1997]. The offshore boundary condition for the modulated energy balance is obtained from individual spectral densities, $G_{\eta\eta}(f_i, \alpha_i)$, within the offshore frequency directional incident wave spectrum

$$\hat{E}_{w,o} = \rho g \sqrt{G_{\eta\eta,o}(f_1, \alpha_1), G_{\eta\eta,o}(f_2, \alpha_2) df d\alpha}, \tag{15}$$

where the subscript o denotes offshore boundary at the 8 m array. Solving for the modulated short-wave energy, equation (12), the corresponding cross-shore distribution of modulated short-wave amplitude is given by

$$\hat{A}_{model}\left(x, f_1, f_2, k_{y,1}, k_{y,2}\right) = \frac{1}{2}\sqrt{\frac{8\hat{E}_w\left(x, f_1, f_2, k_{y,1}, k_{y,2}\right)}{\rho g}}. \tag{16}$$

[21] Consistent with the radiation stress formulation, equation (11), solutions for the VLF motions are assumed to be periodic in t and y

$$\eta\left(x, y, t, f_1, f_2, k_{y,1}, k_{y,2}\right) = \frac{1}{2}\hat{\eta}\left(x, f_1, f_2, k_{y,1}, k_{y,2}\right) \cdot \exp\left[i\left(2\pi \Delta f t - \Delta k_y y\right)\right] + *, \tag{17}$$

where the complex amplitude $\hat{\eta}$ varies in x only. With similar expressions for $\hat{u}$ and $\hat{v}$, substitution into the continuity and momentum equations, equations (2)–(4), yields

$$\hat{\eta} = \frac{-\frac{dh\hat{u}}{dx} - i\Delta k_y h \hat{v}}{i\Delta 2\pi f}, \tag{18}$$

$$\hat{u} = \frac{-g\frac{d\hat{\eta}}{dx} - \hat{F^x}}{i\Delta 2\pi f + \mu}, \tag{19}$$

$$\hat{v} = \frac{ig\Delta k_y \hat{\eta} - \hat{F^y}}{i\Delta 2\pi f + \mu}, \tag{20}$$

where the functional dependencies (x, y, t, f_1, f_2, $k_{y,1}$, $k_{y,2}$) have been dropped for clarity. Substituting equations (19) and (20) into (18), yields

$$h\frac{d^2\hat{\eta}}{dx^2} + \frac{dh}{dx}\frac{d\hat{\eta}}{dx} + \hat{\eta}\left(\frac{\Delta\omega^2}{g} - h\Delta k_y^2 - \frac{i\Delta\omega\mu}{g} - 10^{-4} i\left|\frac{k_y}{hk_{yg}}\right|\right) = -\frac{1}{g}\left(\frac{d}{dx}\left[h\hat{F^x}\right] + i\Delta k_y h\hat{F^y}\right), \tag{21}$$

where the radial frequency $\Delta\omega = 2\pi\Delta f$. In addition to the bottom friction, fifth term on the LHS, a small detuning term (sixth term LHS) has been added to account for edge wave scattering/resonance mismatch induced by the alongshore variability of the topography [*Chen and Guza*, 1998, 1999]. This term affects the edge waves with large alongshore length scales only, $k_y < 0.002\ \mathrm{m}^{-1}$, and has little to no effect on either the VLF response or other edge waves. Terms involving x derivatives of μ were less than 10^{-3} compared with other terms in simulations on the measured bathymetry with rep-

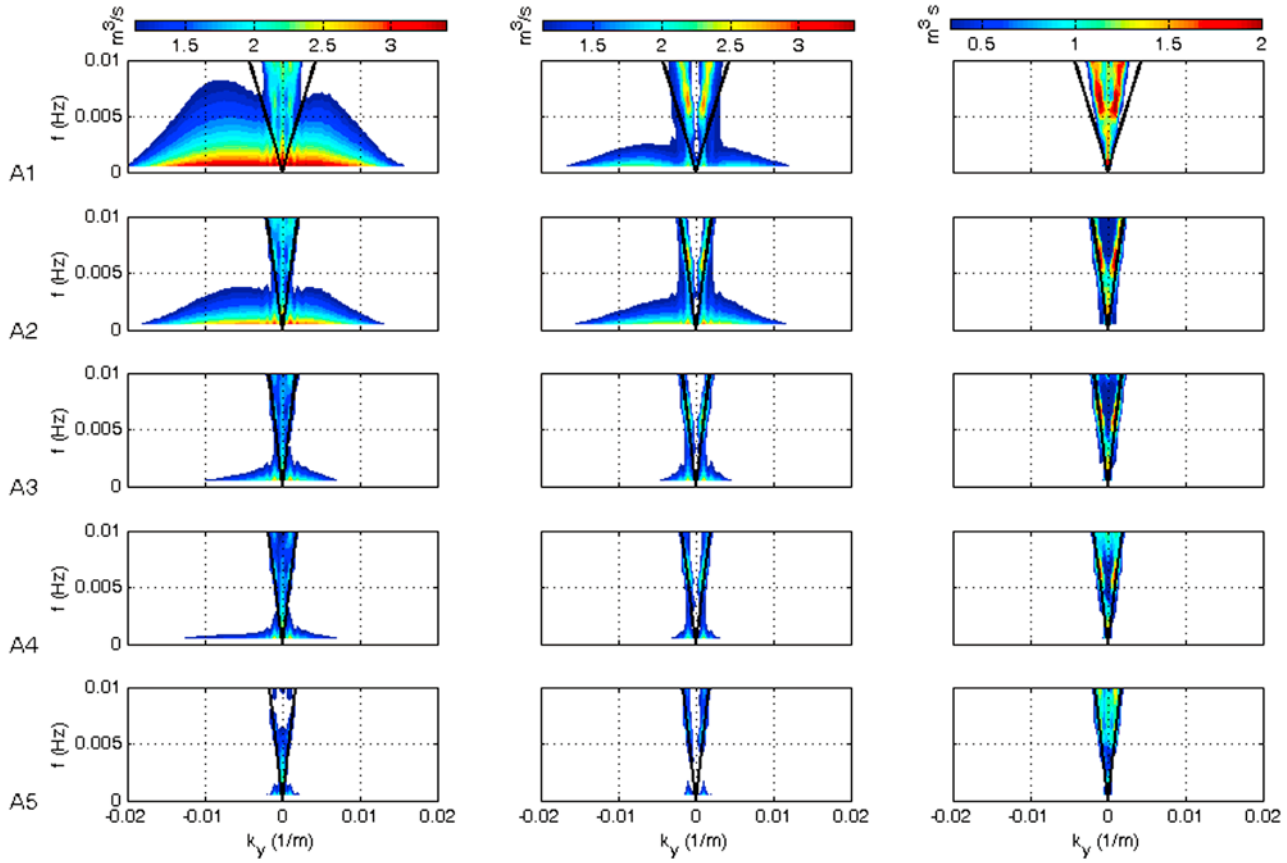

Figure 5. Modeled f-k_y spectra of (left) cross-shore velocity u, (middle) alongshore velocity v, and (right) pressure p for 0400 LT 14 November 1997. Same format as the observations in Figure 2.

resentative typical wave conditions, and are neglected. The boundary conditions for equation (21) are given by a zero flux at the shoreline and a free oblique outgoing (or trapped) motion combined with an incident forced motion offshore. IG motions at the shoreline boundary condition are assumed to reflect, but to avoid singularities, a vertical wall is located in 0.1 water depth (see *Reniers et al.*'s [2002] Appendix B for boundary condition details). VLF results seaward of the shoreline boundary condition are insensitive to a vertical wall located in 0.1 and 0.3 m water depth (not shown).

[22] There are three free model parameters, of which two are associated with the wave breaking model (γ, β) and the third is the bottom friction coefficient c_f. The wave breaking model parameters are set to $\gamma = 0.45$ (depth-limited breaking criteria) and $\beta = 0.05$ (roller dissipation coefficient) based on previous model calibrations at the present field site [*Reniers et al.*, 2002]. c_f is set at a constant value of 0.007, which is consistent for linearized bottom friction estimates used in IG motions [*Reniers et al.*, 2002], shear instability [*Özkan-Haller and Li*, 2003], mean alongshore current model calibrations [*Whitford and Thornton*, 1996], and by alongshore momentum balances of field data [*Church and Thornton*, 1993].

[23] Model computations use all possible pairs made up of the individual short-wave components with energy content larger than 10% of the maximum for an incoming random, directionally spread, incident short-wave field to estimate the total forced IG/VLF response. All individual Δf and Δk_y contributions are summed into equidistant f and k_y spectral bins with a resolution of 0.0005 Hz and 0.001 m^{-1} respectively that are compared to the observed f-k_y spectra. Comparisons of field observation to model results are described below.

5. Model-Field Data Comparisons

[24] Model results are compared with field observations at SandyDuck. The model is forced by the directional spectra measured in 8 meter water depth using the method outlined by *Long and Atmadja* [1994]. Owing to the high degrees of freedom, DOF, the frequency resolution is too coarse to force VLF motions (i.e $\Delta f >$ VLF band) for this model. Therefore, the directional spectra are interpolated to a higher frequency resolution, 0.0005 Hz (see Appendix A).

[25] The modeled f-k_y spectra for 14 November at 0400 LT are qualitatively similar to measured f-k_y spectra (compare Figures 2 and 5). Both model and measured results show an increase in VLF energy density with closer proximity to the shoreline. Consistent with the measurements, the computed VLF energy density is negligible in the surface elevation signal and dominant in the cross-shore motion. The finite alongshore length of the SandyDuck arrays, the low DOF for the spectral estimates, and the extrapolative estimates of the MLE are believed to contribute to the differences in f-k_y

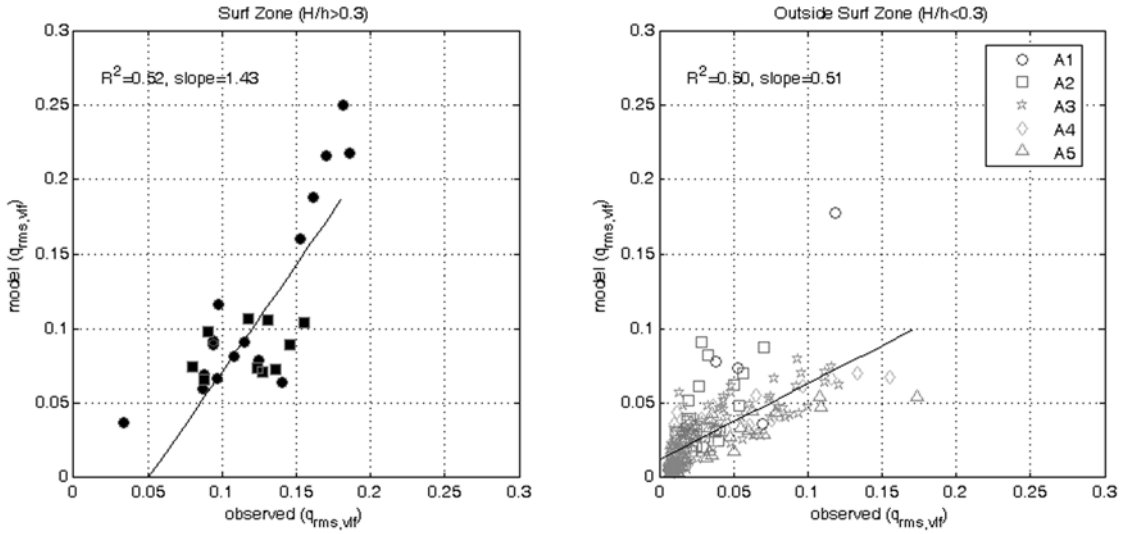

Figure 6. The $q_{RMS,vlf}$ (left) within and (right) seawards of the surf zone ($H_{RMS}/h > 0.3$ and <0.3, respectively) for arrays A1–A5. Linear regression lines are shown, and squared correlations R^2 are given.

spectra between model and measurements. Particularly, since the model alongshore array is alongshore infinite, as it computes energy for all motions in k_y, whereas the field detectable k_y motions are limited by the alongshore extent of the array.

[26] The corresponding cross-shore distribution of $u_{RMS,vlf}$ and $v_{RMS,vlf}$ are similar for model and measurements (Figures 3b and 3c). $u_{RMS,vlf}$ and $u_{RMS,vlf}$ increase to a maximum within the surf zone, shoreward of the innermost measurement array (x = 160 m), and then decrease close to the shoreline. There are no measurements available to evaluate this decay.

[27] To assess the forcing of the VLF motions, the short-wave amplitude modulation within the VLF frequency band (including small infragravity contributions) for field measurements is defined as

$$A_{RMS,vlf} = \sqrt{2\left\langle BP_{0.0005Hz<f<0.004Hz}\left(\left(HP_{f>0.04Hz}(\eta)\right)^2\right)\right\rangle}, \quad (22)$$

where η^2 is the high-pass, *HP*, filtered ($f > 0.04$ Hz), squared, and band-pass, *BP*, filtered (0.0005 Hz < f < 0.004 Hz) sea surface elevation and $\langle\rangle$ denotes time averaging. $\partial A_{RMS,vlf}/\partial x$ is proportional to F^x, but owing to the difficulties in measuring spatial gradients in the field, $A_{RMS,vlf}$ is the best field measurement estimate of forcing to compare with the model showing a favorable match (Figure 3d) where the model equivalent is obtained from the square root of the sum of the squared individual modulated short-wave amplitudes, given by equation (16).

[28] The model and measurements for all 3 h events (Figure 6) indicate that the strongest VLF motions ($q_{vlf,RMS}$ = 0.10–0.20 m/s) occur within the surf zone, while $q_{vlf,RMS}$ outside the surf zone are typically less than 0.10m/s. The model overpredicts $q_{vlf,RMS}$ within the surf zone by approximately 43% and underpredicts $q_{vlf,RMS}$ outside of the surf zone by 50%. Note that only the two inner arrays are within the surf zone for the retained runs.

[29] A measure of the relative fraction of vortical motions over the VLF frequency band is

$$Q_{f-k_y} = \frac{q_{RMS,vlf,vortical}}{q_{RMS,vlf,total}}, \quad (23)$$

where $q_{RMS,vlf,vortical}$ is integrated over the vortical region of f-k_y space, equation (1), and $q_{RMS,vlf,total} = q_{RMS,vlf,vortical} + q_{RMS,vlf,gravity}$ including both gravity and vortical contributions. Averaged over all runs, Q_{f-k_y} is largest (above 0.8) within the surf zone (the inner two arrays) and decreases to about 0.6 at the deepest array (Figure 7).

[30] The similarities between measurements and model results presented above are consistent with previous efforts [e.g., *Fowler and Dalrymple*, 1990] that VLFs are forced by modulations in the short-wave energy within the surf zone.

6. VLF Characteristics

6.1. Uniform Delta Forcing

[31] *Tang and Dalrymple* [1989] found that measured offshore short-wave amplitude modulation, A, in f-k_y spectra displayed broad peaks, which were not strictly located within the VLF band and did not directly correlate with the hydrodynamic response within the surf zone. *Haller et al.* [1999] found that in analyzing SUPERDUCK86 field data coherent wave group forcing was occasionally present but more often absent thus inhibiting a correlation with the observed VLF response. *Reniers et al.* [2004], through numerical modeling, found that directional spreading in short waves results in a broad distribution of amplitude modulation in f-k_y space. However, the computed hydrodynamic response was narrow for both IG and VLF motions, which they attributed to the nonlinear coupling that decreases with increasing Δk_y and Δf. Although the nonlinear coupling of short waves with IG waves has been verified [*Herbers et al.*, 1995], it can not be assumed to give the same response for VLF vortical motions.

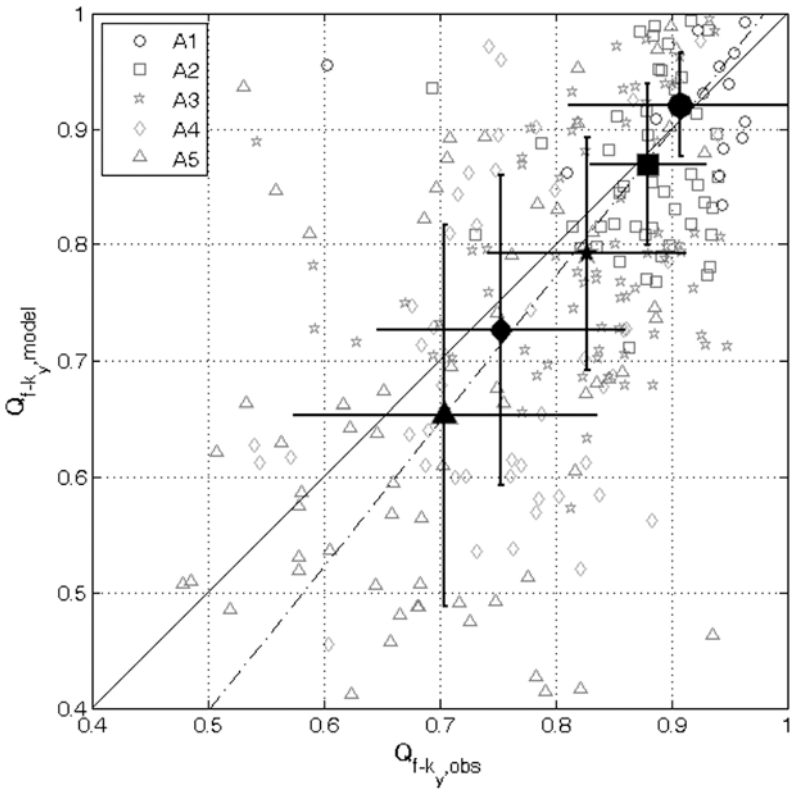

Figure 7. Modeled versus observed relative fraction of vortical motions Q_{f-k_y} (equation (25)). The mean (bold symbols) and standard deviation (bars) are shown for each alongshore array. The dash-dotted line is the linear regression line for mean values for the 5 arrays ($R^2 = 0.98$, $m = 1.25$).

[32] To understand the hydrodynamic response in f and k_y space to uniform forcing, two short waves of equal amplitudes composed of two frequencies and two directions that are equal and opposite are used as input to the model to satisfy the restriction that $\sum S_{xy}(f, \theta) \simeq 0$, so that $V \sim 0$, as observed with field measurements by *Guza et al.* [1986], such that no alongshore current instabilities develop. The uniform delta forcing is realized by keeping the short-wave energy modulation equal for all Δf, Δk_y combinations. The wave group energy for all relevant pairs (Δ) are defined at the 8 m array, where f_2 is fixed at 0.1 Hz and $f_1 < f_2$ with Δf ranging 0.0005–0.02 Hz. Δk_y has a theoretical maximum owing to wave refraction for nonlocally generated short waves. Assuming straight and parallel contours, the Δk_y that can plausibly occur in the surf zone within the vorticity region is limited to

$$|k_{yg}| < \frac{|k_2 \sin(\theta_2) - k_1 \sin(\theta_1)|}{2\pi} < |k_{wry}|, \tag{24}$$

where k_{wry} is the alongshore wave number associated with the theoretical wave refraction (wr) limit. The theoretical limit for the f incident wave angle approaching the shoreline is ±89.9° in deep water (±33° for the selected frequencies at the 8 m array), defined as

$$k_{wry} = \frac{2\pi}{g}\left(f_2^2 + f_1^2\right) = \frac{2\pi}{g}\left(2f_{inc}^2 - 2f_{inc}f_{vlf} + f_{vlf}^2\right). \tag{25}$$

For $f_{vlf} \ll f_{inc}$,

$$k_{wry} = \frac{4\pi}{g} f_{inc}\left(f_{inc} - f_{vlf}\right), \tag{26}$$

where f_{inc} is the incident wave frequency and $f_{vlf} = \Delta f$ is the VLF frequency. Since k_y remains constant in the cross shore for an alongshore homogeneous coast, estimates of k_y in deep water are valid for all depths. k_{wry} decreases with increasing (Δf) and for decreasing incident frequencies (f_{inc}). Waves arriving in the nearshore that were generated in deep water with deep water wave angles of greater than ±89.9° are theoretically not possible. Waves measured locally with nearshore angles that would correspond to equivalent deep water angles of greater than 90° are plausible, but less likely. These waves are generated, not in deep water, but in intermediate water depths on the continental shelf. The analysis only focuses on waves generated in deep water, and ignores regionally generated intermediate waves that can occur at more oblique wave angles.

[33] The model is run with uniform modulated short-wave energy in $\Delta f - \Delta k_y$ space to gain an understanding of the hydrodynamic response. This avoids the added complexity related to a realistic directional wave spectrum where there are multiple short-wave component pairs that contribute to the same $\Delta f - \Delta k_y$ combination (discussed later).

[34] The composite of the uniform delta forcing model runs is shown in Figure 8. Velocity energy density peaks occur within the vorticity region for the VLF band and gravity

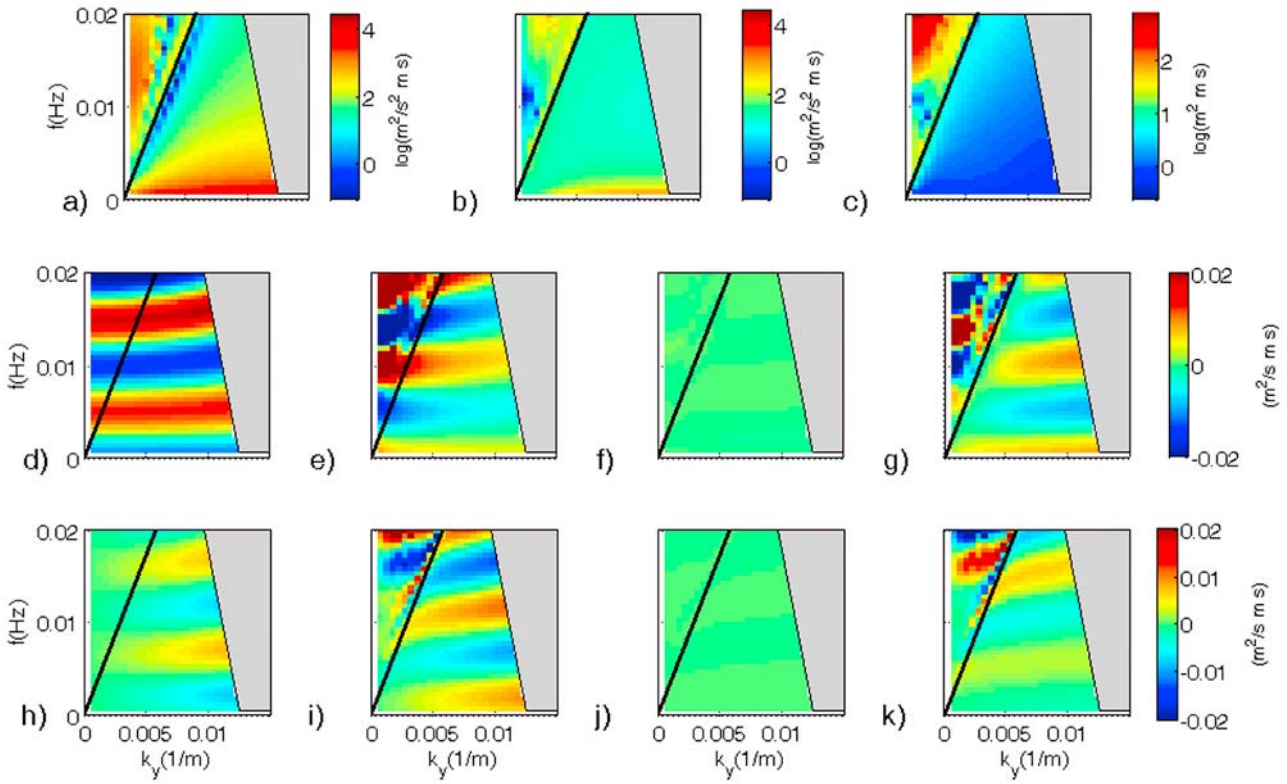

Figure 8. VLF f-k_y spectra at $x = 160$ m obtained by combining results from 3656 model runs with constant input wave group energy at discrete f and k_y components: (a) u, (b) v, (c) η, (d) F^x, (e) $g\frac{d\eta}{dx}$, (f) τ_x, (g) $\frac{du}{dt}$, (h) F^y, (i) $g\frac{d\eta}{dy}$, (j) τ_y, and (k) $\frac{dv}{dt}$. Gray region is the theoretical wave refraction limit (k_{wry}) in 1 m water depth. Solid line represents $k_{yg} = f/\sqrt{gh}$. Color scales are to the right. The f-k_y are symmetric, and only positive k_y is plotted. The alongshore mean beach profile for 30 October 1997 was used.

region for the IG band (Figures 8a and 8b). Energetic peaks occur along the edge-wave dispersion curves, which are a function of frequency directional resolution. Sea surface elevations are mostly contained within the gravity region (Figure 8c).

[35] For the IG motions, the decay of IG energy for increasing $k_y > k_{yg}$ can be attributed to nonlinear coupling [*Herbers et al.*, 1995]. However within the VLF band, for increasing $k_y > k_{yg}$, the velocity response behaves differently than for the IG motions. Both u_{vlf} and v_{vlf} energy density increases with increasing k_y.

[36] Next the momentum balance terms driving the IG and VLF motions are examined (plotting the real part of the complex amplitudes only). The wave forcing for each $\Delta f - \Delta k_y$ combination is initialized at the offshore boundary with a zero phase shift (see Appendix B). F^x is relatively insensitive with respect to k_y at fixed f, and increases with increasing f while changing phase (Figure 8d) (the phase change as a function of f depends on the cross-shore evolution of the Δk_y described in Appendix B). Even though F^x increases at higher frequencies in the vorticity region, the hydrodynamic velocity response spectra decrease owing to the $1/f^2$ dependence (equation (19) and (20) multiplied by their corresponding complex conjugate). Within the vortical region, $g\frac{d\eta}{dx}$ is similar, decreasing with increasing k_y and f, while changing phase with increasing f (Figure 8e). $\frac{du}{dt}$ increases with increasing k_y and changes phase with increasing f (Figure 8g). F^y, $g\frac{d\eta}{dx}$, $\frac{du}{dt}$ increases with increasing k_y and changes phase with increasing f (Figures 8h, 8i, and 8k). τ_x and τ_y have minimal contributions at this location in the cross shore (Figures 8f and 8j).

[37] The k_{wry} intersects the k_{yg} for $f > 0.03$ Hz (Figure 8), limiting vortical motions that are forced by modulations of short waves to lower frequencies with periods longer than 30 seconds. Therefore, the directional components required to generate vortical motions have a relatively small aperture. This constrains the possibilities, such that the alongshore spatial scales range O(50–1000 m) and the temporal scales range from O(200–2000 s).

[38] For a realistic spectrum, all of the relevant short-wave component pairs will generate VLF flow patterns with different spatial scales. The momentum balance associated with the net VLF flow pattern does not illustrate the dynamics of flow patterns owing to constructive and destructive interference (not shown).

6.2. Momentum Balance

[39] The VLF circulation is evaluated for two short-wave components,with frequencies 0.101 Hz and 0.099 Hz respectively and corresponding incidence angles of −12.5° and 12.5°, resulting in a VLF frequency of 0.002 Hz and alongshore wave number of 0.0051 m^{-1} (Figure 9). The resulting VLF flow pattern (Figure 9a) propagates alongshore with a velocity of approximately 0.4 m/s in the positive y direction. The VLF flow pattern spans the surf zone with a smaller countercirculation occurring near the shoreline. The corre-

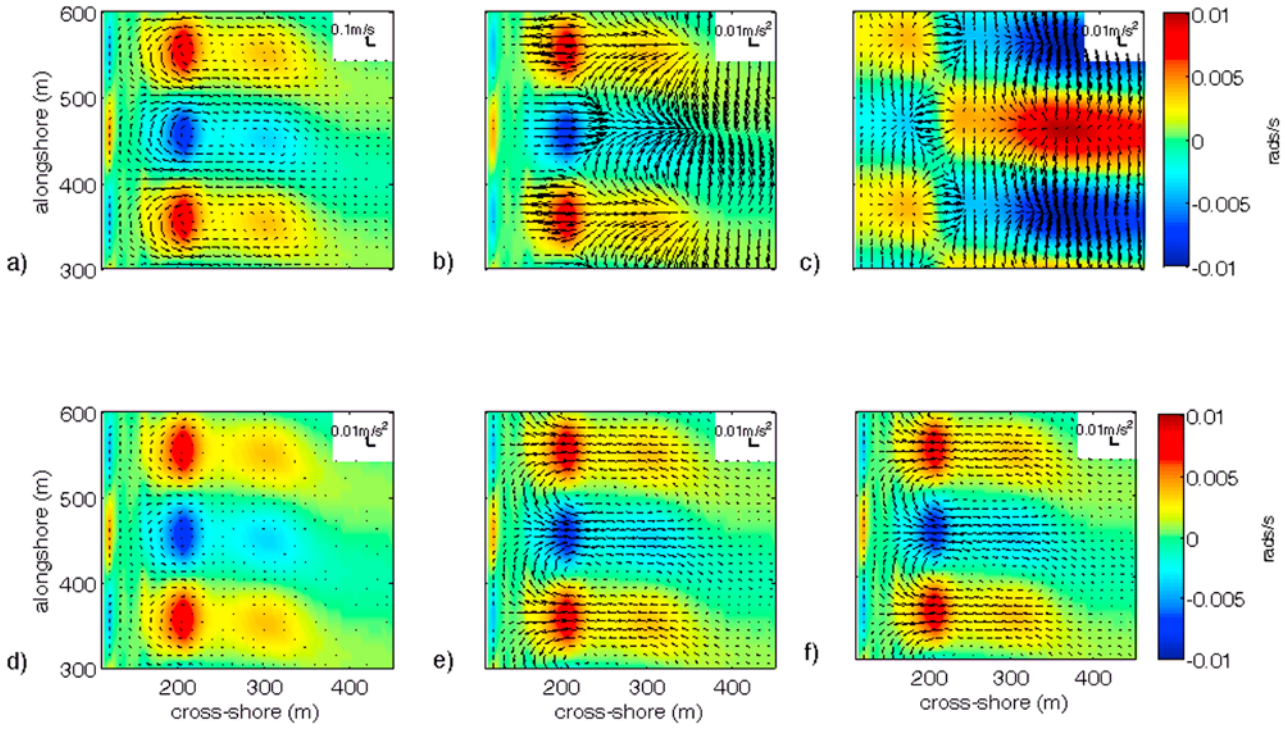

Figure 9. Modeled VLF circulation (black vectors, Figure 9a) and forcing patterns (black vectors, Figures 9b–9e) plotted with vorticity (background color map, Figures 9a, 9b, and 9d–9f) and sea surface elevations (background color map, Figure 9c) as (a) velocity, (b) wave forcing, (c) pressure gradient, (d) bottom shear stress, (e) total forcing, and (f) acceleration. Color scale plotted to the right for vorticity (Figures 9a, 9b, and 9d–9f) and sea surface elevation (Figure 9c).

sponding wave forcing (Figure 9b) shows onshore (offshore) forcing over the area of (positive) negative vorticity, resulting in relatively high (low) setup within the surf zone (Figure 9c). This leads to alongshore and cross-shore pressure gradients, where the latter counteract most of the wave forcing seaward of the surf zone. Note that wave set up and set down are on the order of millimeters, but the cross- and alongshore gradients are significant. Adding the bottom shear stress (Figure 9d) results in the total forcing (Figure 9e) showing an alongshore displacement with the concurrent velocity and vorticity field. This spatial displacement accelerates (decelerates) the flow (Figure 9f) resulting in the alongshore propagation of the velocity/vorticity field. The acceleration (deceleration) results are consistent with the total forcing results such that the total momentum balance sums to zero (not shown).

6.3. SandyDuck 0400 LT 14 November 1997

[40] A measured spectrum for 0400 LT 14 November 2007 is used to construct the forcing to understand the VLF response for realistic waves. The measured directional wave spectrum with $H_{RMS,8m}$ = 1.32 m, T_p = 8.9 s, θ_p = −5.8°, and directional spreading equal to 12° is used to describe the waves at the 8 m offshore boundary. The bathymetry is assumed alongshore homogeneous described by the averaged SandyDuck beach profile for 30 October 2007 (Figure 1b).

[41] The model f-k_y spectral estimates have infragravity motions located on edge-wave dispersion curves for u, v, and η (not shown) within the gravity region. There are energetic regions for the cross- and alongshore velocity components within the vorticity region traveling up and down coast (Figures 10a and 10b). There is more energy traveling in $-k_y$ than $+k_y$, which is associated with the slightly bimodal directional wave spectrum (Figure 10f). Most of the vortical energy is present at the lowest frequency bands for $0.0005 < f < 0.008$ Hz for u, which occurs at slightly higher frequencies than v (Figures 10a and 10b). $G_{uu_{vlf}}$ decreases for increasing $|k_y|$, which is contrary to the decreasing response obtained with the uniform forcing (compare Figure 8d with Figure 10a). The relatively increased $G_{uu_{vlf}}$ at small k_y is related to the modulated short-wave amplitude variance being largest at small k_y values (Figure 10e), and decreasing with increasing k_y and f. This concentration of modulated short-wave amplitude variance at small k_y and f arises from the fact that a directionally spread wave spectrum is biased to wave component pairs with small difference k_y and f. Thus, F^x is largest at small k_y with broad energy (Figure 10c). The dropoff of the short-wave amplitude variance with increasing f (Figure 10e) is weaker than the f dependence of F^x (Figure 8d), resulting in increasing F^x within the vortical region at higher frequencies (Figure 10c). Still, the velocity response is minimal above 0.004 Hz (Figure 10a), given the much stronger f^{-2} dependence of the VLF velocity response (Figure 8a). $G_{vv_{vlf}}$ has energetic regions that peak at $k_y = \pm 0.002$ m^{-1} (Figure 10b), which correspond to the F^y distribution (Figure 10d). The energetic f-k_y regions associated with v and F^y occur as a combination of the concentration of modulated short-wave amplitude variance (Figure 10e) and the k_y dependence of F^y, i.e., increasing for increasing k_y (Figure 8h). Hence, even though the modulated short-wave variance is large at small k_y (Figure 10e), the F^y is minimal

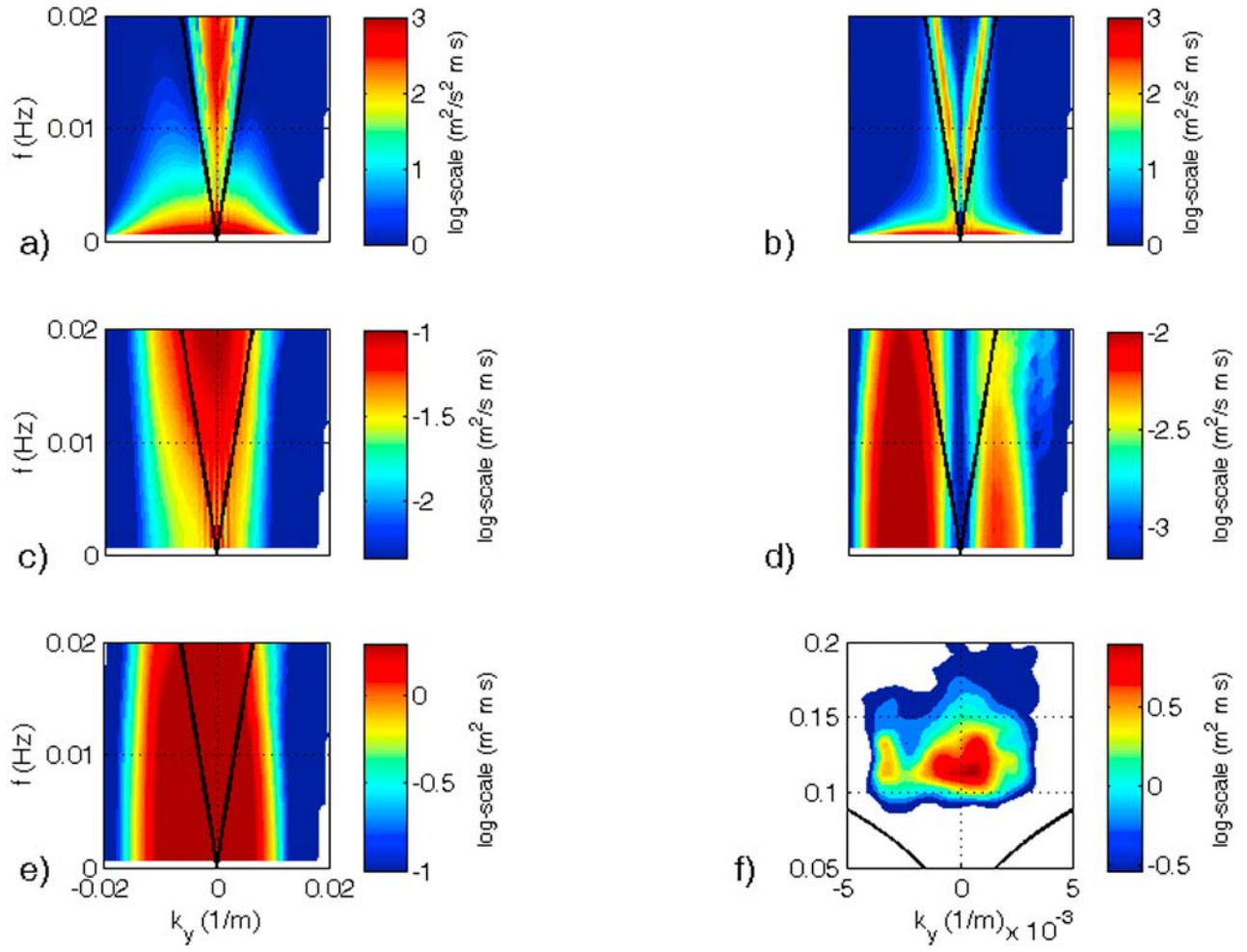

Figure 10. VLF modeled f-k_y spectra at x = 160 m for 0400 LT 14 November: (a) u, (b) v, (c) F^x, (d) F^y, (e) A, and (f) directional spectrum at the 8 m array.

(Figure 8h). As k_y increases, the modulated short-wave variance decreases but not as rapidly as F^y increases with k_y for uniform forcing (Figure 8h), causing a local k_y maximum in $G_{vv_{vlf}}$ (Figure 10d). At larger k_y, the modulated short-wave variance is reduced (Figure 10e), and even though F^y increases with increasing k_y (Figure 8h), this results in decreased values in v and F^y (Figure 10b). Note that there is no energy for f = 0 Hz, because mean motions are not forced with this model.

[42] In summary, the computed VLF velocity response is a result of the concentration of modulated short-wave amplitude variance and corresponding forcing, which both vary as a function of k_y and f. For the realistic SandyDuck case (0400 LT 14 November 1997), the VLF response is limited to very low frequencies and to $|k_y| < 0.015$ m^{-1}. The modulated short-wave energy occurs in both the vorticity and gravity regions, which decreases with increasing k_y and f, similar to the observations by *Tang and Dalrymple* [1989] and *Haller et al.* [1999] and numerical results by *Reniers et al.* [2004]. Energetic spectral modulated short-wave variance (Figure 10e) are found in the vortical region at frequencies above 0.004 Hz, but they do not force a significant vortical response (Figures 10a and 10b) owing to the f^{-2} dependence. Sea surface spectral energy is mostly contained within the gravity region.

[43] The 14 November 2007 at 0400 LT spectrum was evaluated for c_f = 0.1, 0.01, and 0.001. There is less than a 25% difference for $u_{RMS,vlf}$ and a 15% difference for $v_{RMS,vlf}$ between c_f = 0.1 and 0.001 in the surf zone. $u_{RMS,vlf} > v_{RMS,vlf}$ within the surf zone.

6.4. VLF Frequency Limits

[44] Averaged, normalized by variance, frequency spectral estimates for cross- and alongshore velocities and sea surface elevation were computed for both model and measurements (Figure 11) at the five alongshore arrays [x = 160, 210, 260, 310, 385 m] when $V < 25$ cm/s and $H_{RMS,8m} > 0.5$ m to assist in defining the VLF frequency limits. The VLF lower frequency limit is set at 0.0005 Hz owing to the minimum resolvable frequency resolution for the minimal degrees of freedom (10) for 3 h of field measurements and to exclude tidal effects on surf zone currents [*Thornton and Kim*, 1993]. There is a drop in spectral energy density around 0.004Hz (vertical dashed line Figure 11). At higher frequencies, located in the IG band, nodal structure is present representative of cross-shore standing low-mode leaky and edge waves.

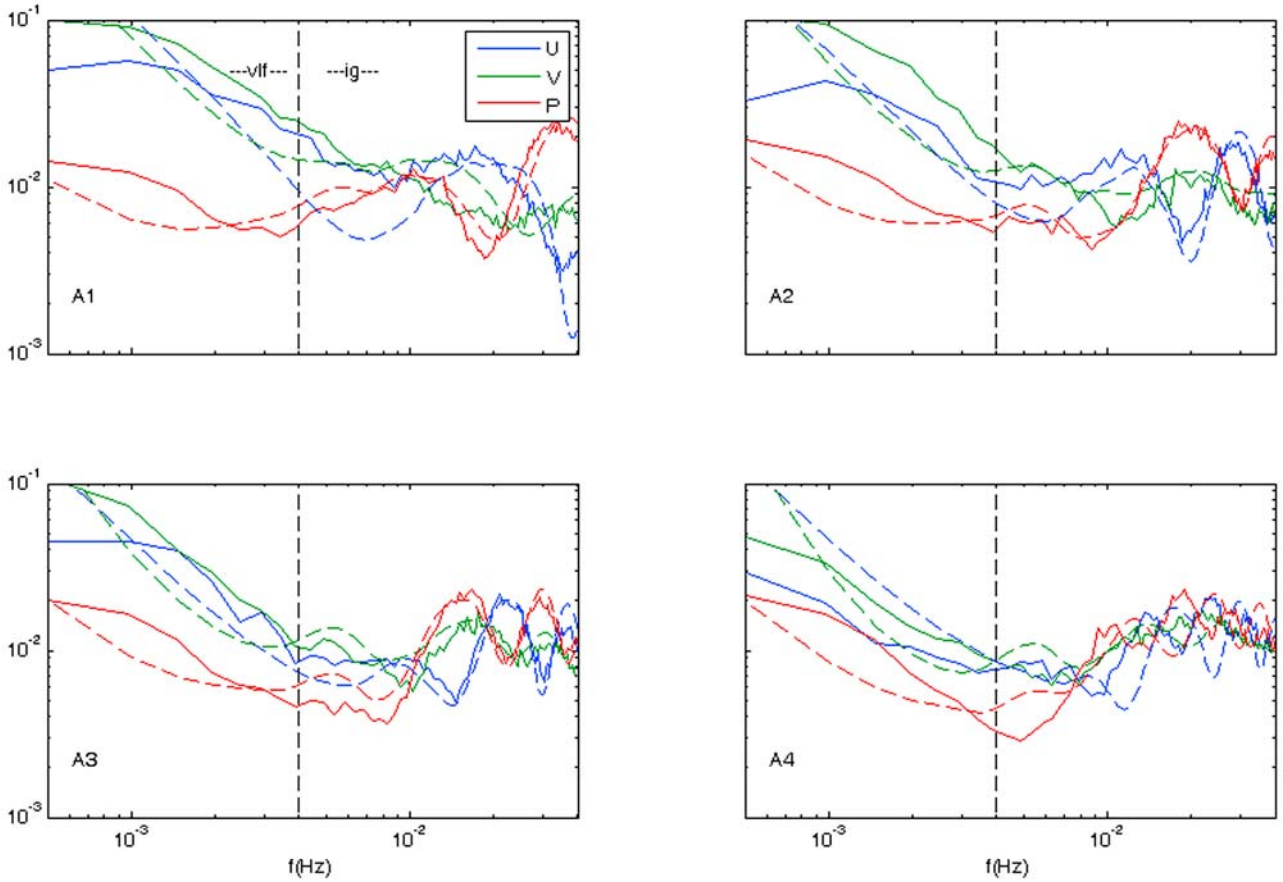

Figure 11. Observed (solid curves) and modeled (dashed curves) normalized frequency spectral estimates for the cross- (blue) and alongshore (green) velocities and pressure (red) in the cross shore at the four alongshore arrays (A1–A4) at SandyDuck for all cases with $V < 25$ cm/s and $H_{RMS,8m} > 0.5$ m. Vertical dashed line represents the suggested frequency division between VLF and IG motions.

At lower frequencies ($f < 0.004$ Hz), the velocity components increase in intensity, while η, as measured by hydrostatic pressure, p, increases slightly or remains relatively constant. This is consistent with both model and measurements. The model velocity energy continues to increase with decreasing frequencies, whereas the field observations level off. The difference between model and measurements increase with decreasing f. The largest difference occurs at A2. These differences may arise in that the model spectral energy assumes an infinite time series and the field observations are limited to 3 h. Other difference may be related to nonlinearities [*Johnson and Pattiaratchi*, 2006] discussed below.

[45] For the inner array (x = 160 m), $G_{uu}(f)$ decreases as $1/f^2$ until $f = 0.004$ Hz, whereas $G_{vv}(f)$ decreases until $f = 0.0035$ Hz. Owing to the small frequency differences in the upper limit and the fact that u_{vlf} is more energetic than v_{vlf}, the upper VLF frequency limit is set at 0.004Hz. Estimates of $q_{RMS,vlf}$ used these frequency limits, which further support the notions that this band is predominantly composed of vortical motions (Figure 3) and is an appropriate frequency limit for VLFs during SandyDuck.

7. Nonlinear Terms: Delft3D Comparison

[46] The present modeling approach ignores the effects of nonlinearity on the generation and evolution of the VLF motions. Nonlinear model results [*Johnson and Pattiaratchi*, 2006; *Reniers et al.*, 2004, 2007; *Long and Özkan-Haller*, 2009] suggest that VLF vortices can interact and travel offshore, thus transferring VLF energy to the outer surf zone or beyond. This offshore flux of VLF energy is likely to be associated with a combination of the nonlinear eddy-eddy interactions, the life time of the eddies, which is subject to bottom friction, viscous damping, and adverse wave forcing [*Reniers et al.*, 2004; *Terrile and Brocchini*, 2007; *Long and Özkan-Haller*, 2009], and the underlying topography such as rip channels [*Brocchini et al.*, 2004; *Kennedy et al.*, 2006; *Reniers et al.*, 2007], barred beaches [*Buhler and Jacobson*, 2001; *Reniers et al.*, 2004] or planar beaches [*Johnson and Pattiaratchi*, 2006]. To qualify the importance of nonlinear effects on the generation and spatial distribution of the VLF's at SandyDuck, calculations were performed using nonlinear Delft3D model described by *Reniers et al.* [2004]. The wave group modulation was similar for linear and nonlinear models. To avoid excessive forcing of modulated short-wave motions close to the waterline, a linear taper was applied reducing the modulation starting at two meter water depth. Calculations were performed for 14 November at 0400 LT, corresponding to the most energetic case with an offshore wave height of 1.4 m. Using a constant tidal elevation (in accordance with the linear model approach), the VLF response

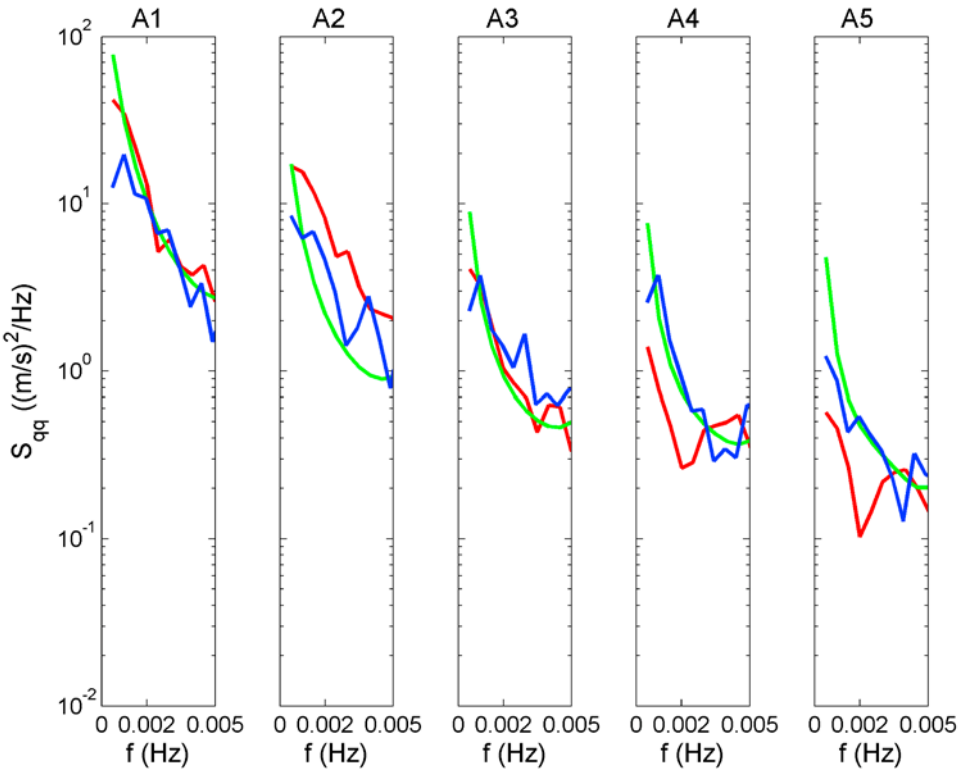

Figure 12. Spectral frequency comparison for14 November 1997 at 0400 LT for the 5 alongshore array (A1–A5) for the field observations (red), the linear model described herein (green), and Delft3D model (blue).

was calculated and analyzed over a period of approximately 3 h. The VLF energy density frequency spectra at the 5 alongshore arrays are intercompared (Figure 12). Both nonlinear and linear model results show similar trends with offshore decaying VLF intensities consistent with the observations. There is no evidence of underestimating the offshore flux of VLF intensity by the linear model for this case, nor are the differences between the model calculated spectra and the observations larger for the linear model.

[47] The corresponding k_y spectra (Figure 13) show that the linear model consistently overestimates the energy density at the smallest VLF wave numbers, which is subsequently compensated by the underestimation at larger alongshore wave numbers. This behavior is absent in the nonlinear results, which show a much broader distribution of the VLF energy density not unlike the observations. The latter may be due to the nonlinear eddy-eddy interactions leading to a transfer of energy to smaller length scales, the self-propagation of eddies to deeper water or interaction with the incident modulated short waves.

[48] The Delft3D (nonlinear) model [*Reniers et al.*, 2004, 2007] and the linear model are forced by two short-wave components, with frequencies 0.101 Hz and 0.099 Hz respectively and corresponding incidence angles of −12.25° and 12.5°, resulting in a VLF frequency of 0.002 Hz and alongshore wave number of 0.0051 m^{-1}. The computations are similar (compare Figures 14a and 14b with Figures 14c and 14d). The resulting VLF flow pattern propagates alongshore with a velocity of approximately 0.4 m/s. Deviations mainly occur for the cross-shore velocity, which is stronger (weaker) during offshore (onshore) flow, associated with nonlinear flow contraction (divergence) that is absent in the linear model. The overall comparison is favorable supporting the present linear model computations of a directly forced VLF response.

[49] In conclusion, the intercomparison between linear and nonlinear VLF energy density spectra show good correspondence with the trends in the observed spectra, however differences at individual frequencies and alongshore wave numbers can be significant. The effect of nonlinearity for the present case seems to manifest itself mostly in the alongshore wave number spectra and not in the frequency spectra nor in the offshore transfer of VLF intensity. The latter may be related to the fact that for the present case waves are breaking at all the alongshore arrays and consequently direct wave group forcing is dominant, which is well captured with the linear modeling effort (Figure 3). During more moderate conditions where waves are breaking at the inner arrays only, offshore advection is expected to become relatively more important (Figure 6 (right)). Although nonlinearity plays a roll in the evolution of the VLF motions, the nonlinear model calculations support the linear model results and the latter gave skillfull predictions for the VLF frequency spectra and corresponding VLF intensities during SandyDuck.

8. Discussion

[50] It has been shown, both in the measurements and model results, that the VLF response is dominated by vortical motions. Consequently the corresponding surface elevation

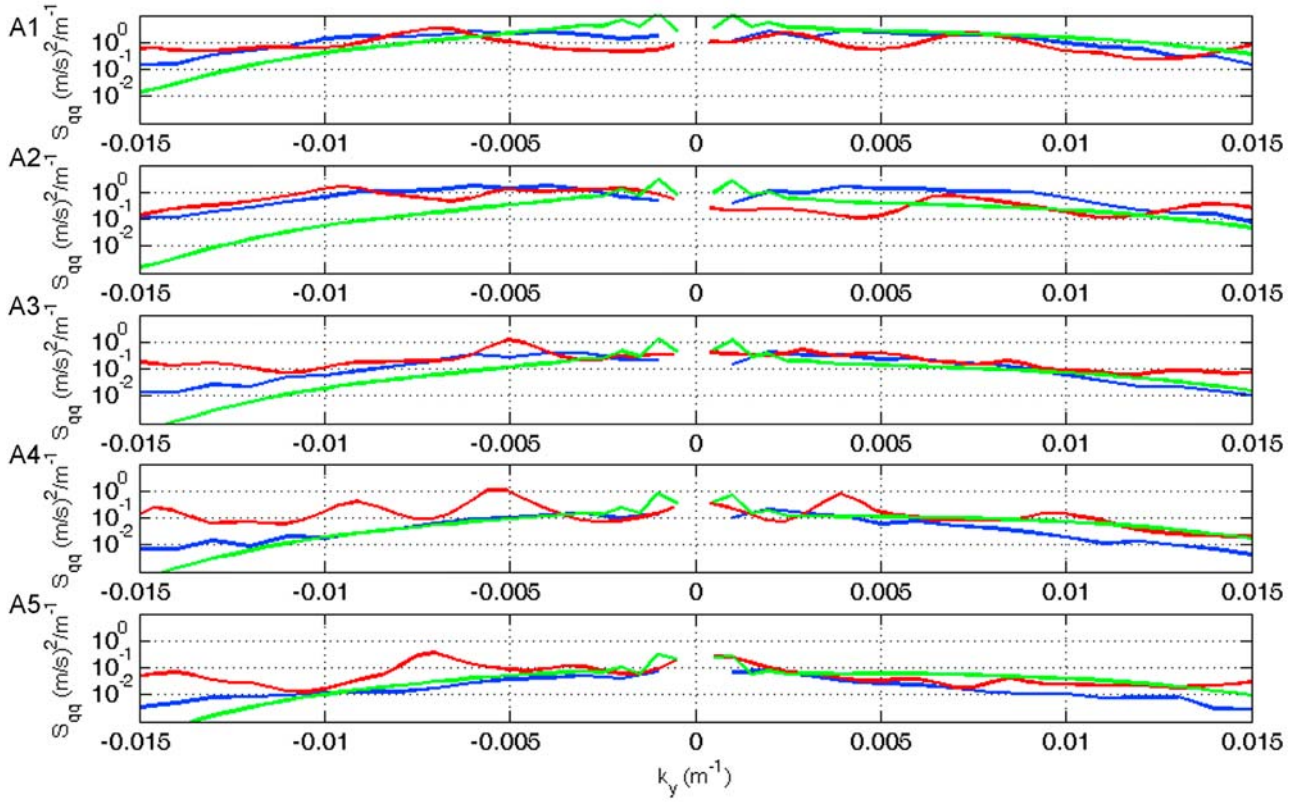

Figure 13. VLF k_y spectral (integrated over 0.0005–0.004 Hz) comparison for 14 November 1997 at 0400 LT for the 5 alongshore arrays (A1–A5) for the field observations (red), the linear model described herein (green), and Delft3D model (blue).

amplitude is small compared with surface elevation amplitude associated with (infra)gravity waves. However, this does not imply that the surface elevation is not important for the VLF response. In fact, the force balance (Figure 9) shows that the pressure forcing is comparable with the radiation stress. In a more general sense, a small setup difference within the surf zone can induce significant pressure-driven nearshore currents [e.g., *Putrevu et al.*, 1995; *Reniers*, 1999; *Chen et al.*, 1999; *Haas et al.*, 2003], provided there is time for the flow to build up [*Van Dongeren*, 1997]. If this time is short, the resulting flow does not develop, similar to a boundary layer motion. However, if the time-scale is large, the flow motion can attain significant velocity amplitudes. This conceptual picture is consistent with the observations that for similar forcing, only the lowest frequencies show significant energy density for comparable forcing.

[51] In the present modeling approach we considered forced VLFs only, ignoring self-advection, nonlinear VLF interactions and episodic forcing at the incident wave time scale. These processes could mask the broad VLF response in k_y space due to direct forcing, and potentially explain the peaks in the observed spectra that are absent in the model results (compare Figures 2 and 5). However, a recent study by *Long and Özkan-Haller* [2009] showed that the VLF velocity field in absence of shear instabilities consists predominantly of forced VLFs (consistent with the present modeling approach). In addition, the nonlinear time domain calculations presented here, which allow for self-advection and nonlinear interactions, show mostly a broadening of the k_y spectrum by moving energy from large scale VLF motions to smaller scale VLF features resulting in a broad(er) spectrum without discrete peaks (Figure 13). Hence, an alternative explanation for the peaks in the observed VLF spectra is associated with the relative sparseness (in time and space) of observation points at the alongshore arrays. This also forms the rationale behind the use of the MLE [*Regier*, 1975] instead of the more commonly applied Iterative maximum likelihood estimator (IMLE) [*Pakwa*, 1983; *Oltman-Shay and Guza*, 1987], where the application of the latter can easily result in the enhancement of spurious spectral peaks. Note that the broad VLF response is different from the response obtained for shear instabilities which reside on a narrow f-k_y ridge associated with their propagation by the alongshore current [e.g., *Oltman-Shay et al.*, 1989] for which the IMLE is well suited.

9. Summary and Conclusions

[52] Energetic vortical surf zone motions that predominantly reside within the very low frequency band ($0.0005 < f < 0.004$ Hz; $k_y < 0.02$ m^{-1}) in f-k_y space were observed in the field on a weakly pronounced double-barred beach at Duck, NC, when the alongshore currents were minimal. A linear spectral hydrodynamic model that is nonlinearly forced by directionally spread short waves inducing spatial and temporal gradients in radiation stresses and pressure is used to examine the hydrodynamic response inside and outside of the surf zone. The linear model facilitates a method of evaluating

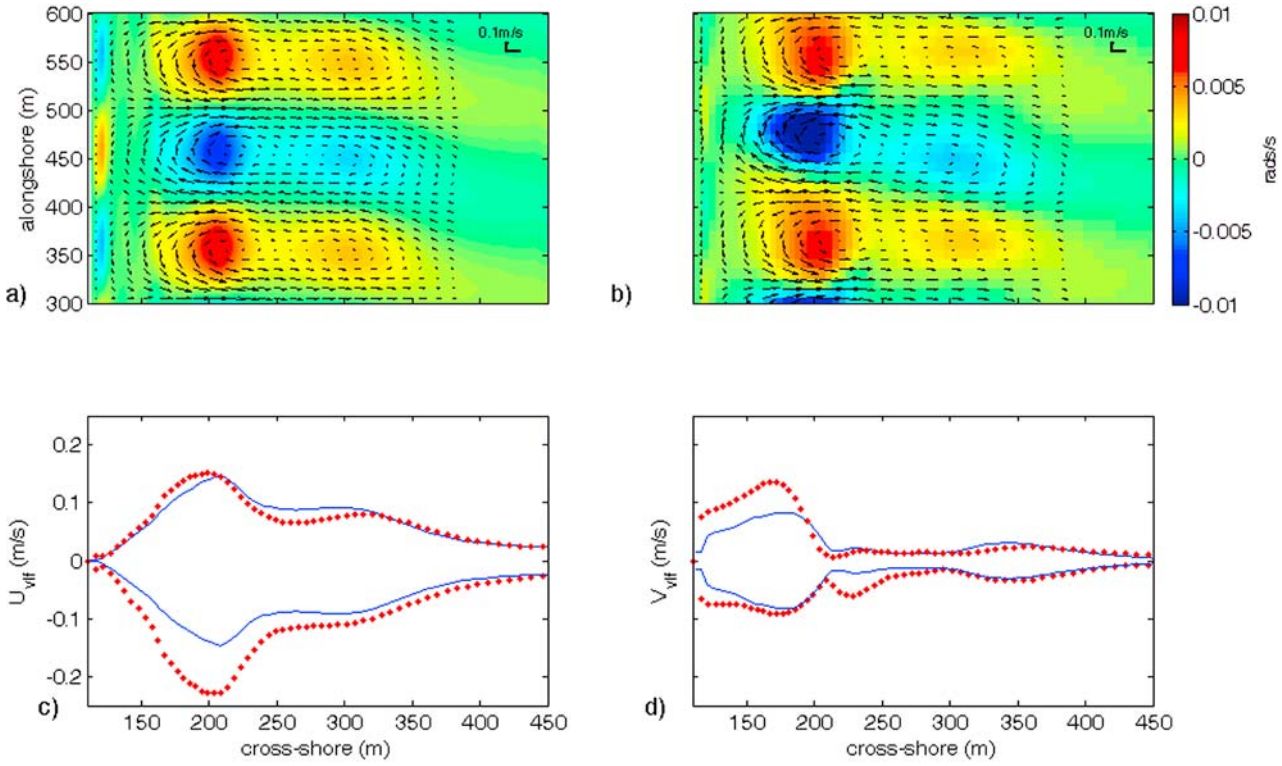

Figure 14. (a) Linear model results for VLF flow field (arrows) and vorticity (background color map) forced by two short-wave components, $f_1 = 0.101$ Hz, $f_2 = 0.099$ Hz, and incidence angles (in 8 m water depth) $\theta_1 = -12.25°$, and $\theta_2 = 12.5°$, resulting in a VLF frequency 0.002 Hz and alongshore wave number 0.0051 m^{-1}. (b) Similar for nonlinear (Delft3D) model results. Color scale for vorticity is in s^{-1}. The envelope of (c) u_{vlf} and (d) v_{vlf} for linear model (blue line) and nonlinear model (red dots) versus cross-shore location x.

the mechanisms responsible for the VLF generation. It is harder to decouple these mechanisms with a nonlinear model, as both instabilities and direct forcing exist. Though nonlinearities are important, the linear model compares well with the field observations of VLFs. The linear model is used to define the VLF vortical characteristics. VLFs have the spatial scales of O(1 surf zone width) in the cross shore, O(50–1000 m) in the alongshore, and the temporal scale of O(200–2000 s), which slowly propagate (O(10 cm/s)) in the alongshore. The seaward-directed flow is O(20 cm/s), which decreases quickly seaward of the surf zone. Although both observed and modeled VLF pressure fluctuations are relatively weak, the model momentum balance suggests that VLF pressure gradients are as important as the modulated short-wave forcing by sea and swell in the VLF velocity response. Model calculations further underpin the conclusion that the VLF-f-k_y response is a function of wave group forcing associated with the frequency directional distribution of the incident sea and swell spectra. The strongest response is found at the lowest VLF frequencies. This is due to the fact that the modulated short-wave forcing and pressure gradients have more time to accelerate the VLF flow field in combination with the highest modulated short-wave amplitude variance in the forcing.

[53] The ubiquitousness of edge waves on various beaches was not documented until coherent alongshore arrays were deployed in the field at various locations [*Huntley et al.*, 1981; *Oltman-Shay and Guza*, 1987]. Here we show that the directional spreading at the short waves is responsible for the observed VLFs at SandyDuck. Since directionally spread short waves are ubiquitous, then VLFs are ubiquitous.

Appendix A: High-Resolution Directional Wave Spectra

[54] The offshore boundary condition for the energy balance is obtained from individual spectral density components, $G_{\eta\eta}(f_i, \alpha_i)$, from offshore frequency directional spectra, where the energy is defined as

$$\hat{E}_{w,o}(\triangle f, \triangle k_y) = \rho g \sqrt{G_{\eta\eta}(f_1, \alpha_1) G_{\eta\eta}(f_2, \alpha_2)} df d\alpha. \qquad \text{(A1)}$$

Therefore, if the resolution of the frequency directional wave spectra is too coarse, motions in the VLF will not be resolved ($\triangle f > 0.004$ Hz). In general, most frequency directional wave spectra, in particular the FRF array located in 8 m water depth, are estimated with 160 DOFs resulting in a df of 0.0097 Hz, which is too coarse to evaluate VLF motions. Hence, the frequency directional spectrum is interpolated to 0.0005 Hz, which is the minimum resolvable resolution for p,u, and v measurements with a minimum 10 DOFs based on a 3 h record. Higher resolution directional spectra were computed at the 8 m array, resulting in 16 DOFs and a $df = 0.00097$ Hz.

The model results from the interpolated directional spectra and the high-resolution spectra compared well, with the interpolated directional spectra providing smoother results and $u_{RMS,vlf}$ differed by less than 5%. The interpolated directional spectra are used in this manuscript.

Appendix B: Forcing Estimates

[55] Owing to the difficulty in computing accurate estimates of spatial derivatives of the radiation stress gradients in f-k_y space with the SandyDuck arrays, an alternative estimate of nonlinear forcing is required to compare the model and measurements. VLFs are forced by spatial gradients in modulated short-wave radiation stresses, defined in the cross shore [*Reniers et al.*, 2002] as

$$\hat{S}_{xx} = \left(\hat{E}_w\left[n\left(\cos^2\theta + 1\right) - \frac{1}{2}\right] + \hat{E}_r\left[2\cos^2\theta\right]\right) \cdot \exp\left[-i\int \triangle k_x dx + \phi_0\right], \tag{B1}$$

$$\hat{S}_{xy} = \left(\hat{E}_w \sin\theta\cos\theta + \hat{E}_r[2\cos\theta\cos\theta]\right)\exp\left[-i\int \triangle k_x dx + \phi_0\right], \tag{B2}$$

$$\hat{S}_{yy} = \left(\hat{E}_w\left[n\left(\sin^2\theta + 1\right) - \frac{1}{2}\right] + \hat{E}_r\left[2\sin^2\theta\right]\right) \cdot \exp\left[-i\int \triangle k_x dx + \phi_0\right], \tag{B3}$$

where n is the shoaling coefficient, $\frac{C_g}{C}$, and $\hat{S}_{xx}$, $\hat{S}_{xy}$, and $\hat{S}_{yy}$ are functions of short-wave energy modulation, $\hat{E}_w$ and roller energy modulation $\hat{E}_r$. The phase of the cross-shore modulation of the wave and roller energy depends on the evolution of the cross-shore wave number difference, $\triangle k_x$, made up by the two incident wave components forming the wave group and a random phase, ϕ_0. The short-wave energy modulation is defined as, $\hat{E}_w = \frac{1}{2}\rho g\hat{A}^2$, where A is the wave envelope amplitude. Note that $\hat{E}_r$ is a function of $\hat{E}_w$. Therefore, changes in radiation stress are related to changes in wave envelope amplitude, $F_x = \frac{1}{\rho h}\left(\frac{\partial S_{xx}}{\partial x} + \frac{\partial S_{xy}}{\partial y}\right)$, hence, the transformation of A may be considered a proxy for F. This is consistent with modeling mean surf zone motions, such as alongshore currents [e.g., *Thornton and Guza*, 1986; *Reniers and Battjes* 1997] and rip currents [e.g., *Bowen*, 1969].

[56] **Acknowledgments.** We dedicate this manuscript to memory of Howell Peregrine and his vision of surf zone vortical motions. We thank Bob Guza, Steve Elgar, Tom Herbers, and Britt Raubenheimer for providing the field observations, sponsored by the Office of Naval Research. Kent Hathaway and Chuck Long collected the 8 m array data. Jim Noyes generously provided a compendium of processed data results. The authors appreciate the constructive comments and valuable scientific input provided by Bob Guza and Steve Elgar. We appreciate the valuable comments by anonymous reviewers for making this a better manuscript. JM was funded by ONR N000140510154, N000140510352, N0001407WR20226, N0001408WR20006, and the National Science Foundation (NSF) OCE 0728324. AR was funded by ONR under contracts N000140310829 and N000140710556 and NSF funding OCE 0754426. Additional funding for AR was provided by the Dutch National Science Foundation (NWO) contract DCB.5856, the University of Miami and Delft University. Accessibility and permission to use data provided by the Field Research Facility of the US Army Engineer Waterways Experiment Station's Coastal Engineering Research Center is appreciated very much.

References

Bowen, A. J. (1969), Rip currents: 1. Theoretical investigations, *J. Geophys. Res.*, *74*, 5467–5478.

Brocchini, M., A. B. Kennedy, L. Soldini, and A. Mancinelli (2004), Topographically-controlled, breaking wave-induced macrovortices. 1: Widely separated breakwaters, *J. Fluid Mech.*, *507*, 289–307.

Buhler, O., and T. E. Jacobson (2001), Wave-driven currents and vortex dynamics on barred beaches, *J. Fluid Mech.*, *449*, 313–339.

Chen, Q., R. A. Dalrymple, J. T. Kirby, A. B. Kennedy, and M. C. Haller (1999), Boussinesq modeling of a rip current system, *J. Geophys. Res.*, *104*, 20,617–20,637.

Chen, Y. Z., and R. T. Guza (1998), Resonant scattering of edge waves by longshore periodic topography, *J. Fluid Mech.*, *369*, 91–123.

Chen, Y. Z., and R. T. Guza (1999), Resonant scattering of edge waves by longshore periodic topography: Finite beach slope, *J. Fluid Mech.*, *387*, 255–269.

Church, J. C., and E. B. Thornton (1993), Effects of breaking wave induced turbulence within a longshore current model, *J. Coastal Eng.*, *20*, 1–28.

Elgar, S., R. T. Guza, W. C. O'Reilly, B. Raubenheimer, and T. H. C. Herbers (2001), Wave energy and direction observed near a pier, *J. Waterw. Port Coastal Ocean Eng.*, *127*, 2–6.

Feddersen, F., and R. T. Guza (2003), Observations of nearshore circulation: Alongshore uniformity, *J. Geophys. Res.*, *108*(C1), 3006, doi:10.1029/2001JC001293.

Fowler, R. E. (1991), Wave-group forced nearshore circulation: A generation mechanism for migrating rip currents and low frequency motion, *Res. Rep. CACR-91-03*, Cent. for Appl. Coastal Res., Univ. of Del., Newark, Del.

Fowler, R. E., and R. A. Dalrymple (1990), Wave-group forced nearshore circulation, in *Proceedings of the 22nd International Conference on Coastal Engineering*, pp. 729–742, Am. Soc. of Civ. Eng., Delft, Netherlands.

Guza, R. T., and E. B. Thornton (1985), Observations of surf beat, *J. Geophys. Res.*, *90*, 3161–3171.

Guza, R. T., E. B. Thornton, and N. Christensen Jr. (1986), Observations of steady longshore currents in the surf zone, *J. Phys. Oceanogr.*, *16*(11), 1959–1969.

Haas, K. A., I. A. Svendsen, M. C. Haller, and Q. Zhao (2003), Quasi-three-dimensional modeling of rip current systems, *J. Geophys. Res.*, *108*(C7), 3217, doi:10.1029/2002JC001355.

Haller, M. C., U. Putrevu, J. Oltman-Shay, and R. A. Dalrymple (1999), Wave group forcing of low frequency surf zone motion, *Coastal Eng.*, *41*, 121–136.

Herbers, T. H. C., S. Elgar, and R. T. Guza (1995), Generation and propagation of infragravity waves, *J. Geophys. Res.*, *100*, 24,863–24,872.

Holman, R. A. (1981), Infragravity energy in the surf zone, *J. Geophys. Res.*, *86*, 6442–6450.

Huntley, D. A., R. T. Guza, and E. B. Thornton (1981), Field observations of surf beat, part I: Progressive edge waves, *J. Geophys. Res.*, *86*, 6451–6466.

Johnson, D., and C. Pattiaratchi (2006), Boussinesq modelling of transient rip currents, *Coastal Eng.*, *53*, 419–439.

Kennedy, A., Q. Chen, J. Kirby, and R. Dalrymple (2000), Boussinesq modeling of wave transformation, breaking and runup, *J. Waterw. Port Coastal Ocean Eng.*, *126*(1), 39–47.

Kennedy, A., M. Brocchini, L. Soldini, and E. Gutierez (2006), Topographically-controlled breaking wave-induced macrovortices. Part 2. Changing geometries, *J. Fluid Mech.*, *559*, 57–80.

Kirby, J., G. Wei, Q. Chen, A. Kennedy, and R. Dalrymple (1998), Funwave 1.0: Fully non-linear Boussinesq wave model documentation and user's manual, *Tech. Rep. CACR-98-06*, Cent. for Appl. Coastal Res., Univ. of Del., Newark, Del.

Lippmann, T. C., T. H. C. Herbers, and E. B. Thornton (1999), Gravity and shear wave contributions to nearshore infragravity motions, *J. Phys. Oceanogr.*, *24*, 231–239.

Long, C. E., and J. Atmadja (1994), Index and bulk parameters for frequency directional spectra measured at CERC Field Research Facility, September 1990 to August 1991, *Misc. Pap. CERC-94-5*, U.S. Army Waterw. Exp. Stn., Vicksburg, Miss.

Long, J. W., and H. T. Özkan-Haller (2009), Low-frequency characteristics of wave group-forced vortices, *J. Geophys. Res.*, *114*, C08004, doi:10.1029/2008JC004894.

MacMahan, J. H., A. J. H. M. Reniers, E. B. Thornton, and T. P. Stanton (2004), Surf zone eddies coupled with rip current morphology, *J. Geophys. Res.*, *109*, C07004, doi:10.1029/2003JC002083.

Munk, W. H. (1949), Surf beats, *Eos Trans. AGU*, *30*, 849–854.

Nairn, R. B., J. A. Roelvink, and H. N. Southgate (1990), Transition zone width and implications for modelling surf zone hydrodynamics, in *Coastal Engineering Conference, 1990: Proceedings of the International*

Conference, edited by B. L. Edge, pp. 68–81, Am. Soc. of Civ. Eng., Reston, Va.

Noyes, T. J., R. T. Guza, S. Elgar, and T. H. C. Herbers (2004), Field observations of shear waves in the surf zone, *J. Geophys. Res.*, *109*, C01031, doi:10.1029/2002JC001761.

Oltman-Shay, J., and R. T. Guza (1987), Infragravity edge wave observations on two California beaches, *J. Phys. Oceanogr.*, *17*, 644–663.

Oltman-Shay, J., P. A. Howd, and W. A. Birkemeier (1989), Shear instabilities of mean longshore current: 2. Field observations, *J. Geophys. Res.*, *94*, 18,031–18,042.

Özkan-Haller, H. T., and Y. Li (2003), Effects of wave-current interaction on shear instabilities of longshore currents, *J. Geophys. Res.*, *108*(C5), 3139, doi:10.1029/2001JC001287.

Pakwa, S. S. (1983), Island shadows in wave directional spectra, *J. Geophys. Res.*, *88*, 2579–2591.

Peregrine, D. H. (1998), Surf zone currents, *Theor. Comput. Fluid Dyn.*, *10*, 295–309.

Peregrine, D. H. (1999), Large-scale vorticity generation by breakers in shallow and deep water, *Eur. J. Mech. B*, *18*, 403–408.

Phillips, O. M. (1977), *The Dynamics of the Upper Ocean*, 2nd ed., 336 pp., Cambridge Univ. Press, New York.

Putrevu, U., J. Oltman-Shay, and I. A. Svendsen (1995), Effect of alongshore non-uniformities on alongshore current predictions, *J. Geophys. Res.*, *100*(C8), 16,119–16,130.

Regier, L. A. (1975), Observations of the power and directional spectrum of oceanic surface waves, Ph.D. dissertation, Univ. of Calif., San Diego, Calif.

Reniers, A. J. H. M. (1999), Longshore current dynamics, Ph.D. dissertation, Delft Univ. of Technol., Delft, Netherlands.

Reniers, A. J. H. M., and J. A. Battjes (1997), A laboratory study of longshore currents over barred and non-barred beaches, *Coastal Eng.*, *30*, 1–22.

Reniers, A. J. H. M., A. R. Van Dongeren, J. A. Battjes, and E. B. Thornton (2002), Linear modelling of infragravity waves during Delilah, *J. Geophys. Res.*, *107*(C10), 3137, doi:10.1029/2001JC001083.

Reniers, A. J. H. M, J. A. Roelvink, and E. B. Thornton (2004), Morphodynamic modeling of an embayed beach under wave-group forcing, *J. Geophys. Res.*, *109*, C01030, doi:10.1029/2002JC001586.

Reniers, A. J. H. M., J. H. MacMahan, E. B. Thornton, and T. P. Stanton (2007), Modeling of very low frequency motions during RIPEX, *J. Geophys. Res.*, *112*, C07013, doi:10.1029/2005JC003122.

Ryrie, S. C. (1983), Longshore motion due to an obliquely incident wave-group, *J. Fluid Mech.*, *137*, 273–284.

Schäffer, H. A. (1993), Infragravity waves induced by short-wave groups, *J. Fluid Mech.*, *247*, 551–588.

Shira, V. I., V. V. Vornovich, and N. G. Kozhelupova (1997), Explosive instability of vorticity waves, *J. Phys. Oceanogr.*, *27*, 542–554.

Stive, M. J. F., and H. J. de Vriend (1994), Shear stresses and mean flow in shoaling and breaking waves, in *Proceedings of the Twenty-Fourth International Conference*, edited by B. L. Edge, pp. 594–608, Am. Soc. of Civ. Eng., Reston, Va.

Tang, E. C.-S., and R. A. Dalrymple (1989), Nearshore circulation: Rip currents and wave groups, in *Nearshore Sediment Transport*, edited by R. J. Seymour, pp. 205–230, Plenum, New York.

Terrile, E., and M. Brocchini (2007), A dissipative point-vortex model for nearshore circulation. *J. Fluid. Mech.*, *589*, 454–477.

Thornton, E. B., and R. T. Guza (1986), Surf zone longshore currents and random waves: Field data and models, *J. Phys. Oceanogr.*, *16*, 1165–1178.

Thornton, E. B., and C. S. Kim (1993), Longshore current and wave height modulation at tidal frequency inside the surf zone, *J. Geophys. Res.*, *98*, 16,509–16,519.

Tucker, M. J. (1950), Surfbeats: Sea waves of 1 to 5 minutes period, *Proc. R. Soc. London A*, *202*, 565–573.

Van Dongeren, A. R. (1997), Quasi 3D-modeling of nearshore hydrodynamics, *Rep. CACR-94-04*, 234 pp., Cent. for Appl. Coastal Res., Univ. of Del., Newark, Del.

Wei, G., J. T. Kirby, S. T. Grilli, and R. Subraymanya (1995), A fully nonlinear Boussinesq model for surface waves. Part I. Highly nonlinear unsteady waves, *J. Fluid Mech.*, *294*, 71–92.

Whitford, D. J., and E. B. Thornton (1996), Bed shear stress coefficients for longshore currents over a barred profile, *Coastal Eng.*, *27*, 243–262.

J. H. MacMahan and E. B. Thornton, Oceanography Department, Naval Postgraduate School, Spanagel Hall, Monterey, CA 93943, USA. (jhmacmah@nps.edu)

A. J. H. M. Reniers, Rosenstiel School of Marine and Atmospheric Science, University of Miami, 4600 Rickenbacker Cswy., Miami, FL 33149, USA.